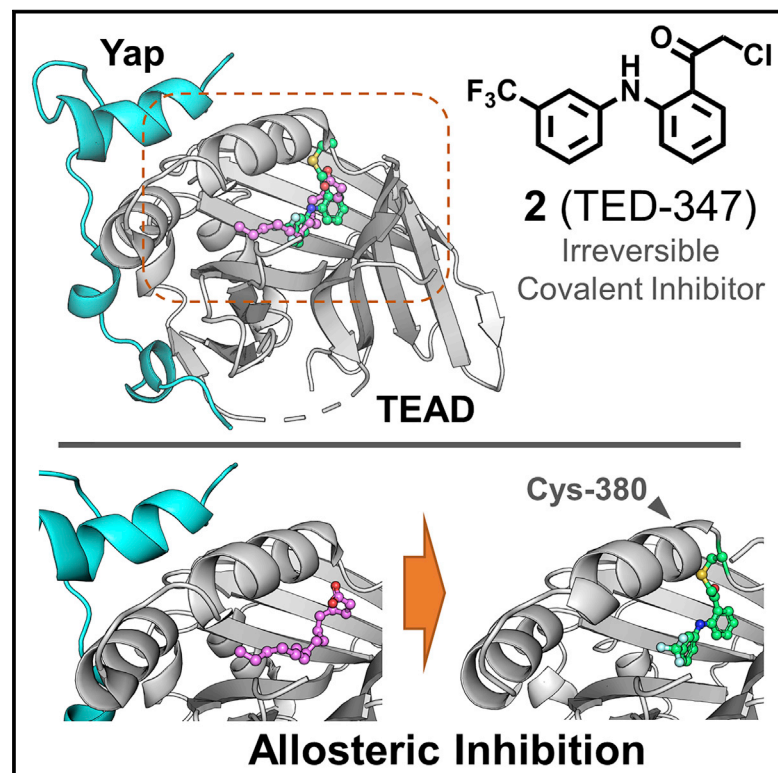


Cell Chemical Biology

Small-Molecule Covalent Modification of Conserved Cysteine Leads to Allosteric Inhibition of the TEAD·Yap Protein-Protein Interaction

Graphical Abstract



Authors

Khuchtumur Bum-Erdene,
Donghui Zhou,
Giovanni Gonzalez-Gutierrez, ...,
Karen E. Pollok, Clark D. Wells,
Samy O. Meroueh

Correspondence

smeroueh@iu.edu

In Brief

A small molecule that forms a covalent bond with a conserved cysteine within the palmitate binding pocket of TEADs was found to inhibit the TEAD·Yap protein-protein interaction through allostery. The compound inhibited TEAD transcriptional activity in mammalian cells and blocked patient-derived glioblastoma cell viability.

Highlights

- Small molecules form a covalent bond with palmitate cysteine
- Covalent engagement of cysteine inhibited TEAD4·Yap1 protein-protein interaction
- Inhibition of TEAD4·Yap1 in mammalian cells blocked TEAD transcriptional activity
- Small-molecule inhibition of TEAD4·Yap1 inhibited glioblastoma cell viability

Small-Molecule Covalent Modification of Conserved Cysteine Leads to Allosteric Inhibition of the TEAD•Yap Protein-Protein Interaction

Khuchtumur Bum-Erdene,¹ Donghui Zhou,¹ Giovanni Gonzalez-Gutierrez,² Mona K. Ghazayel,¹ Yubing Si,¹ David Xu,³ Harlan E. Shannon,⁴ Barbara J. Bailey,⁴ Timothy W. Corson,^{1,5} Karen E. Pollok,⁴ Clark D. Wells,¹ and Samy O. Meroueh^{1,6,*}

¹Department of Biochemistry and Molecular Biology, Indiana University School of Medicine, Indianapolis, IN 46202, USA

²Department of Molecular and Cellular Biochemistry, Indiana University, Bloomington, IN 47405, USA

³Department of BioHealth Informatics, Indiana University School of Informatics and Computing, Indianapolis, IN 46202, USA

⁴Department of Pediatrics, Herman B. Wells Center for Pediatric Research, Indiana University Simon Cancer Center, Indiana University School of Medicine, Indianapolis, IN 46202, USA

⁵Eugene and Marilyn Glick Eye Institute, Department of Ophthalmology, Indiana University School of Medicine, Indianapolis, IN 46202, USA

⁶Lead Contact

*Correspondence: smeroueh@iu.edu

<https://doi.org/10.1016/j.chembiol.2018.11.010>

SUMMARY

The Hippo pathway coordinates extracellular signals onto the control of tissue homeostasis and organ size. Hippo signaling primarily regulates the ability of Yap1 to bind and co-activate TEA domain (TEAD) transcription factors. Yap1 tightly binds to TEAD4 via a large flat interface, making the development of small-molecule orthosteric inhibitors highly challenging. Here, we report small-molecule TEAD•Yap inhibitors that rapidly and selectively form a covalent bond with a conserved cysteine located within the unique deep hydrophobic palmitate-binding pocket of TEADs. Inhibition of TEAD4 binding to Yap1 by these compounds was irreversible and occurred on a longer time scale. In mammalian cells, the compounds formed a covalent complex with TEAD4, inhibited its binding to Yap1, blocked its transcriptional activity, and suppressed expression of connective tissue growth factor. The compounds inhibited cell viability of patient-derived glioblastoma spheroids, making them suitable as chemical probes to explore Hippo signaling in cancer.

INTRODUCTION

The Hippo signaling pathway controls tissue homeostasis and organ size (Wu et al., 2003). Hippo is triggered by an NF2/Merlin-Kibra-Expanded tumor suppressor complex that activates the Ste20-like kinase, Hippo (Mst1/2 in mammals), which then phosphorylates and activates the large tumor suppressor kinases (Lats1/2). Lats1/2 kinases, in turn, phosphorylate the transcriptional co-activators Yap and TAZ to promote their cytoplasmic retention and degradation (Yu and Guan, 2013). Lack of cell crowding coupled with mechanical loading such as stretching, location at edges of an epithelial sheet, or stiffness of the sur-

rounding extracellular matrix are factors that promote Yap/TAZ (Aragona et al., 2013) to enter the nucleus where they co-activate TEA domain (TEAD) transcription factors (Hong and Guan, 2012; Mauviel et al., 2012; Pobbati and Hong, 2013; Yu and Guan, 2013). In mammals, there exist four highly conserved TEAD (also known as TEF) transcription factors, namely TEAD1–4 (Eldridge et al., 1997). The average sequence identity among TEADs is 73%, which is considered high (Noland et al., 2016). TEADs possess similar domains: an N-terminal DNA binding TEA/ATTS domain (Anbanandam et al., 2006) and a C-terminal immunoglobulin-like β -sandwich fold (Pobbati et al., 2012). TEADs alone cannot initiate gene expression; they rely on co-activators such as Yap and its paralog TAZ, as well as vestigial-like proteins (VGLL), and the p160 family of nuclear receptor co-activators (Hong and Guan, 2012; Pobbati and Hong, 2013). Activation of TEADs initiates expression of CCN matricellular growth factors, such as connective tissue growth factor (CTGF), Cyr61, epidermal growth factor receptor ligand amphiregulin, and Axl receptor tyrosine kinase (Fridell et al., 1996; Mauviel et al., 2012; Piccolo et al., 2013; Rosell et al., 2013; Yu et al., 2012). Expression of these growth factors leads to cell growth, apoptotic avoidance, and stem cell self-renewal (Hong and Guan, 2012; Piccolo et al., 2013; Yu and Guan, 2013).

Despite substantial evidence that Yap1 promotes tumor progression and metastasis through its TEAD-interaction domain (Liu-Chittenden et al., 2012; Zhao et al., 2008), no small molecules have been identified that directly disrupt this interaction. The approved drug verteporfin, which was identified by high-throughput screening to impair Hippo signaling (Liu-Chittenden et al., 2012), has not been demonstrated to physically associate with either TEAD or Yap. Instead, recent work indicates that verteporfin works through other mechanisms, including the inhibition of p62 (Donohue et al., 2014; Donohue et al., 2013; Donohue et al., 2011). Cyclic Yap-like peptides (Zhou et al., 2015) and recombinant proteins such as VGLL have been used to disrupt the interaction of TEAD with Yap1 *in vitro*. VGLL, which directly competes with Yap1 for a common binding site on TEAD, was also found to negatively regulate TEAD/Yap activity and to suppress lung and gastric tumor activity (Zhang et al., 2014). Along these

lines, a peptide that mimics the TDU domain of VGLL4 was found to suppress tumor growth in gastric cancer cells both *in vitro* and *in vivo* (Jiao et al., 2014). Small interfering RNA-lipid nanoparticles that target Yap1 have also been shown to decrease liver tumor proliferation (Fitamant et al., 2015). While upstream regulators of Hippo signaling such as G-protein-coupled receptors and kinases are amenable to small-molecule inhibition (Fan et al., 2013; Reddy and Irvine, 2013; Yu et al., 2012), their prominence in other signaling pathways will likely result in off-target effects.

The three-dimensional structure of the TEAD·Yap complex (Chen et al., 2010; Li et al., 2010) reveals that disruption of the protein-protein interaction is expected to be difficult. The interaction interface between TEAD·Yap is unusually large, exceeding 1,000 Å² (Chen et al., 2010). It is devoid of a well-defined druggable binding pocket. The large interface and lack of binding site likely explains the failure to develop agents that competitively inhibit the TEAD·Yap interaction. Alternatively, a deep hydrophobic palmitate binding pocket within all TEAD members has been shown to be important for their stability but not their biological activity (Chan et al., 2016; Noland et al., 2016). All TEAD paralogs are palmitoylated at a conserved cysteine located within this pocket (Noland et al., 2016). Considering that the palmitate pocket is located away from the TEAD·Yap interface, it has been suggested that palmitoylation allosterically alters TEAD to stabilize an interaction with Yap (Chan et al., 2016; Noland et al., 2016). Thus, targeting the palmitate binding pocket may be an effective strategy for modulating the interaction of TEAD with Yap.

Here we report the discovery of small molecules that bind to the TEAD4 palmitate pocket, form a covalent bond with a conserved cysteine, and disrupt the TEAD4·Yap1 protein-protein interaction. Starting with the structure of flufenamic acid bound to TEAD2 (Pobbati et al., 2015), we designed a small molecule that can form a covalent bond with a conserved cysteine within the palmitate-binding pocket. Extensive explicit-solvent molecular dynamics simulations revealed that covalent bond formation of this compound reduced the TEAD4·Yap1 binding affinity. Synthesis of this compound and several derivatives followed by biochemical studies that characterized binding affinity and inhibition kinetics confirmed the computational results. The structure of the covalent complex between TEAD and compounds was revealed by X-ray crystallography. Compounds were explored for their effect on TEAD4 protein-protein interactions and transcriptional activity in HEK-293 mammalian cells, as well as in glioblastoma (GBM) cancer cell lines.

RESULTS

Molecular Dynamics Simulations Reveal that Covalent Bond Formation at Allosteric Pocket Cysteine Reduces TEAD4·Yap1 Affinity

The TEAD three-dimensional structure contains a 12-strand β -sandwich fold, flanked by four short α helices (Figure 1A). The N-terminal region of Yap1 (residues 61–100) forms an α helix (residues 61–73), which binds between TEAD α 3 and α 4 helices, and an Ω loop (residues 85–99), which binds near TEAD α 1 and β 12 (Figure 1A). Crystal structures of TEADs reveal the presence of a deep hydrophobic pocket that is occupied by palmitate (Figure 1B) (Pobbati et al., 2015). The Food and Drug Administration

(FDA)-approved drug flufenamic acid **1** (TED-346) was previously found to bind weakly to two sites on TEAD2, but did not inhibit TEAD binding to Yap (Pobbati et al., 2015). One of the binding sites is located within the deep hydrophobic palmitate-binding pocket of the transcription factor and the other at the protein-protein interaction interface. The binding mode of **1** (TED-346) in the deep pocket of TEAD2 shows that the compound's carboxylic acid moiety is located near the thiol of a conserved cysteine residue (Cys-380) that is the acylation site of a palmitoyl group (Chan et al., 2016). We hypothesized that modification of the carboxylic acid to an electrophile may lead to covalent bond formation and modulation of the TEAD4·Yap1 protein-protein interaction. Considering that the palmitate pocket is located outside the TEAD4·Yap1 protein-protein interaction interface, it was not obvious whether adduct formation would stabilize or inhibit the TEAD4·Yap1 protein-protein interaction. To explore the effect of adduct formation on the TEAD4·Yap1 interaction, we designed a derivative of compound **1**, namely **2** (TED-347), which possesses a chloromethyl ketone moiety that can form a covalent bond with Cys-367. We applied microsecond explicit-solvent molecular dynamics simulations to determine whether covalent bond formation at the cysteine residue affects TEAD4·Yap1 protein-protein interaction. We carried out three separate simulations: TEAD4·Yap1, [TEAD4·**2**]·Yap1 non-covalent complex (Figure 1C), and [TEAD4·**2**]·Yap1 covalent complex (Figure 1D). Each simulation consisted of 50 separate 50-ns trajectories resulting in 2.5 μ s (50 \times 50 ns) of explicit-solvent molecular dynamics simulations per complex. Structures sampled from these simulations were collected to determine the free energy of binding of TEAD4 to Yap1 using the widely used MM-GBSA free energy calculation method (Figure 1E). We found that non-covalent binding of **2** (TED-347) to TEAD4 exhibited little change to the TEAD4·Yap1 binding affinity ($\Delta\Delta G_{\text{MMGBSA}} = 0.5 \pm 0.1$ kcal/mol). However, covalent bond formation of **2** (TED-347) to TEAD4 led to substantially greater loss of TEAD4 affinity to Yap1 by nearly 10.9 ± 0.1 kcal/mol (Figure 1F). The 20-fold reduction in the binding affinity suggests that adduct formation at Cys-367 leads to allosteric inhibition of the TEAD4·Yap1 protein-protein interaction. These results were confirmed by repeating the calculations with compound **5** (TED-551). Non-covalent binding of the compound led to little change for the affinity of the TEAD4·Yap1 complex ($\Delta\Delta G_{\text{MMGBSA}} = -0.5 \pm 0.1$ kcal/mol), while covalent bond formation led to substantial reduction in the MM-GBSA binding affinity to 5.3 ± 0.1 kcal/mol (Figure 1F). These results suggest that mere binding to the pocket is not sufficient to disrupt the protein-protein interaction, whereas covalent bond formation with the cysteine residue may lead to inhibition of the interaction.

Compound **2** and Derivatives Form a Covalent Bond at an Allosteric Site Cysteine and Inhibit TEAD4 Binding to Yap1

Chloromethyl ketone **2** (TED-347) (Figure 2) was prepared to determine whether it formed a covalent complex with TEAD4. To explore direct binding of the compounds to TEAD4, we developed a fluorescence polarization (FP) assay that used a fluorescently labeled Yap1-derived peptide FAM-YAP_{60–99} (FAM-DSETDLEALFNVMNPKTANVPQTVPMLRKLPSFCKPP). FAM-YAP_{60–99} includes the entire Yap1·TEAD4 binding interface (Figure 3A). The labeled peptide binds to TEAD4 with a K_D

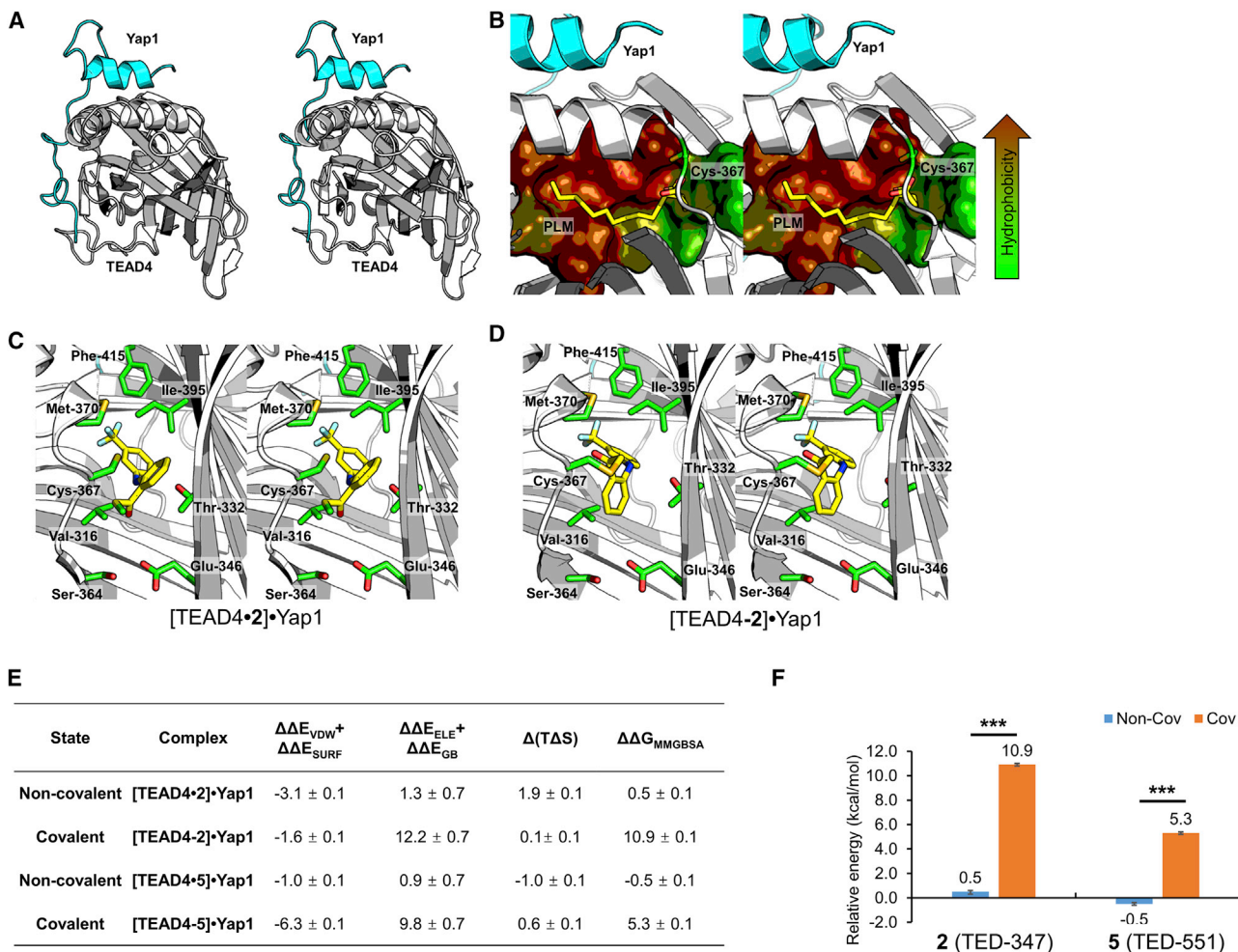


Figure 1. Three-Dimensional Structures and Free Energy Calculations

(A) Stereo view of the X-ray structure of the TEAD4•Yap1 complex (PDB: 3JUA). TEAD4 and Yap1 are shown in gray and cyan ribbon representation, respectively. (B) Structure of the TEAD4•Yap1 complex depicting the deep hydrophobic pocket of TEAD4. The pocket is occupied by palmitate, which is shown as capped sticks and color coded by atom type (yellow and red correspond to carbon and oxygen atoms, respectively). The pocket is shown in solvent-accessible surface area and color coded by hydrophobicity (brown is hydrophobic). PLM corresponds to palmitate.

(C) Non-covalent complex of **2** (TED-347) bound to TEAD4. Compound **2** (TED-347) and surrounding amino acids are shown as capped sticks and color coded by atom type (for **1** [TED-347], yellow, blue, red, cyan, and green correspond to carbon, nitrogen, oxygen, fluorine, and chlorine respectively). Carbon atoms are shown in green and sulfur atoms in gold for TEAD4).

(D) Covalent complex of **2** (TED-347) and TEAD4. Compound **2** (TED-347) and surrounding residues are shown as capped sticks and color coded by atom type (for **1** [TED-347], yellow, blue, red, cyan, and green correspond to carbon, nitrogen, oxygen, fluorine, and chlorine, respectively). Carbon atoms are shown in green and sulfur atoms in gold for TEAD4).

(E) MM-GBSA free energy of binding of Yap1 to TEAD4 bound to compounds **2** (TED-347) or **5** (TED-551). MM-GBSA free energies and their components correspond to the difference between TEAD4•Yap1 with TEAD4 in complex with a compound and TEAD4•Yap1 with TEAD4 in the apo state. All energies are reported in kcal/mol; mean ± SE, n = 30,000 snapshots.

(F) The change in free energy for covalent and non-covalent complexes between TEAD4 and **1** (TED-347); mean ± SE, n = 30,000 snapshots. p values were calculated using two-tailed t tests, ***p < 0.0005.

of 78.2 ± 9.9 nM. Compound **1** (TED-346, flufenamic acid) was tested and we found that the drug did not inhibit the TEAD4•Yap1 interaction, consistent with previous studies (Figure 3B). The effects of other compounds on the TEAD4•Yap1 interaction were tested using our FP assay. Following 24 hr incubation of TEAD4 with **2** (TED-347) at 4°C, the compound inhibited the TEAD4•Yap1 protein-protein interaction by 53% with an apparent EC_{50} of 5.9 ± 0.4 μ M (Figure 3B). Compound **3** (TED-550) did not inhibit, as the compound cannot form a co-

valent bond, since the chlorine atom leaving group is replaced by a methyl group (Figure 3B). A time-dependent study was performed at 0.5, 6, 24, and 48 hr for **2** (TED-347) (Figure 3C), whereby **2** (TED-347) reached maximum inhibition of 80% at 48 hr. Based on the time- and concentration-dependent inhibition study of TEAD4 with **2** (TED-347) (Figure 3D), the rates of inactivation were calculated for the compounds and several derivatives (Table S1). The maximum rate of inactivation of **2** (TED-347) was calculated to be 0.038 ± 0.003 hr^{-1} (Figure 3D),

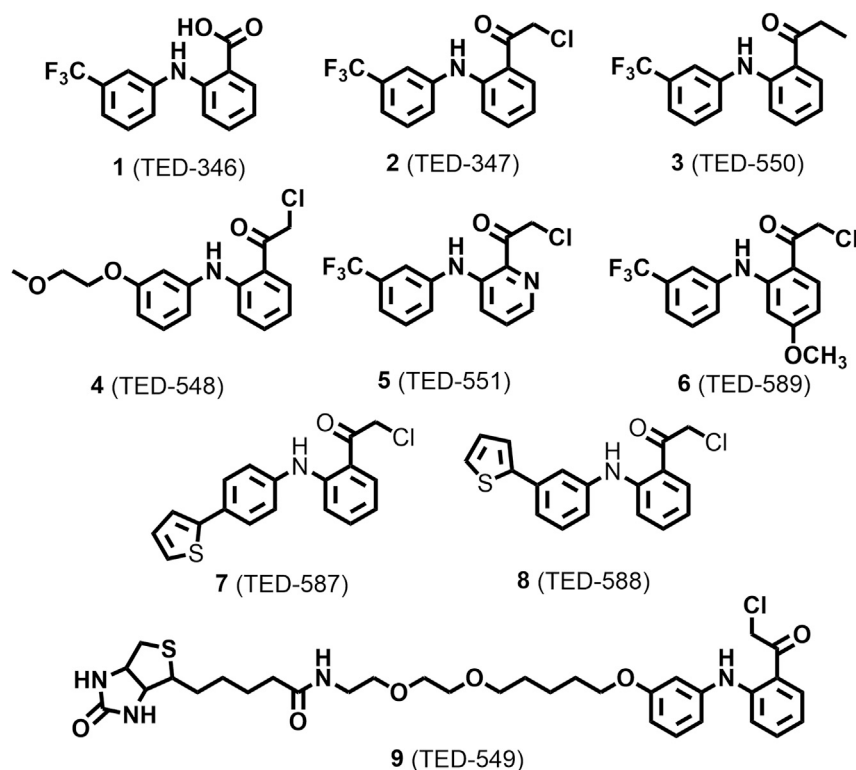


Figure 2. Structures of Compounds

347), as well as peak broadening, compared with the TEAD4 incubated with DMSO, both of which suggest conformational change of the protein. Furthermore, it is highly unlikely that Cys-367 oxidation is responsible for the lack of 100% inhibition at longer times, since we have shown that covalent bond formation is rapid and complete within less than an hour. Also, whole-protein mass spectrometry carried out at 24 hr does not reveal the presence of the oxidized species.

To further establish that **2** (TED-347) specifically forms a bond with Cys-367 within the central pocket of TEAD4, we tested its interaction with a TEAD4 Cys367Ser mutant. Adduct formation by **2** (TED-347) to the mutant TEAD4 Cys367Ser was analyzed by mass spectrometry. After 24 hr, **2** (TED-347) did not form an adduct with the mutant protein (Figure 4A). TEAD4 Cys367Ser mutant showed no change in affinity for FAM-YAP₆₀₋₉₉ peptide, with a K_D of $49.1 \pm$

3.0 nM (Figure 4B). Subsequently, the compounds were tested for inhibition of the peptide binding to TEAD4 Cys367Ser mutant. We found that **2** (TED-347) did not inhibit the mutant TEAD4 Cys367Ser protein binding to the peptide, suggesting that covalent bond formation by **2** (TED-347) is essential for its ability to inhibit the protein-protein interaction (Figure 4C).

We explored whether mere covalent bond formation with conserved Cys-367 was sufficient to inhibit the TEAD4·Yap1 protein-protein interaction. ESI mass spectrometry was used to detect formation of adducts by iodoacetamide. In 30 min, we saw a concentration-dependent adduct formation up to 200 μ M, whereby the protein was modified by a single adduct (Figure S1A). After 6 hr, the protein was modified by a single adduct at all concentrations of iodoacetamide (Figure S1B). We did not see the presence of a second reaction site until 24 hr at the highest tested concentration of 200 μ M (Figure S1C). To determine whether Cys-367 is the target of the single adduct, we reacted TEAD4 Cys367Ser mutant with varying concentrations of iodoacetamide for 24 hr. After 24 hr there was no modification of the protein except for a small adduct that was detected only at 200 μ M iodoacetamide concentration, which is consistent with the wild-type TEAD4 (Figure S1D). Although iodoacetamide is able to react with TEAD4 Cys-367, it was unable to inhibit the activity of the protein in the FP assay (Figure S1E). Thus, merely reacting with the cysteine does not guarantee inhibition of activity.

corresponding to a $t_{1/2}^{\infty}$ of 18.2 hr. To determine whether **2** (TED-347) is a reversible or irreversible inhibitor, we incubated TEAD4 with 50 μ M compound for 24 hr at 4°C and then dialyzed it against buffer for 24 hr at 4°C, prior to interaction with the fluorescently labeled Yap1 peptide (Figure 3E). Compound **2** (TED-347) inhibited the TEAD4·Yap1 interaction even after dialysis, indicating that the compound is an irreversible inhibitor.

The formation of a covalent bond between compounds and TEAD4 was confirmed by whole-protein electrospray ionization (ESI) mass spectrometry studies. Following incubation of TEAD4 at 10 μ M with 200 μ M of **2** (TED-347) for 24 hr at 4°C, a peak at 26,229 was observed, corresponding to the TEAD4-**2** (TED-347) adduct, while the peak at 25,952 corresponding to TEAD4 disappeared (Figure 3F). As expected, compound **3** (TED-550) only showed a peak at 25,952, indicating no adduct formation. The covalent bond formation by **2** (TED-347) was relatively fast (Figure 3G), reaching nearly 100% adduct formation after 30 min of incubation with TEAD4. Because the rate of inhibition developed over a longer time scale (Figure 3C), **2** (TED-347) is proposed to induce a slow conformational change in TEAD4 that inhibits its interaction with Yap1. To rule out the possibility that **2** (TED-347) induces slow aggregation of TEAD4, and not the proposed slow conformational change, we incubated GST-TEAD4 with DMSO or **2** (TED-347) for 24 hr at 4°C, followed by injection into a size-exclusion chromatography (SEC) column (Figure 3H). There is no significant aggregation of GST-TEAD4 after 24 hr of incubation, with or without **2** (TED-347). There was a slight increase in dimer formation for the TEAD4 sample incubated with **2** (TED-347) compared with the sample incubated with DMSO. In addition, we noticed a slight shift in the retention time of the TEAD4 sample incubated with **2** (TED-

347) inhibited the interaction between TEAD4 and Yap1 peptide observed in our FP assay, we applied biolayer interferometry (BLI) that used full-length Yap1 protein. The binding affinity between glutathione S-transferase (GST)-tagged Yap1 and the TEAD4 protein was found to be

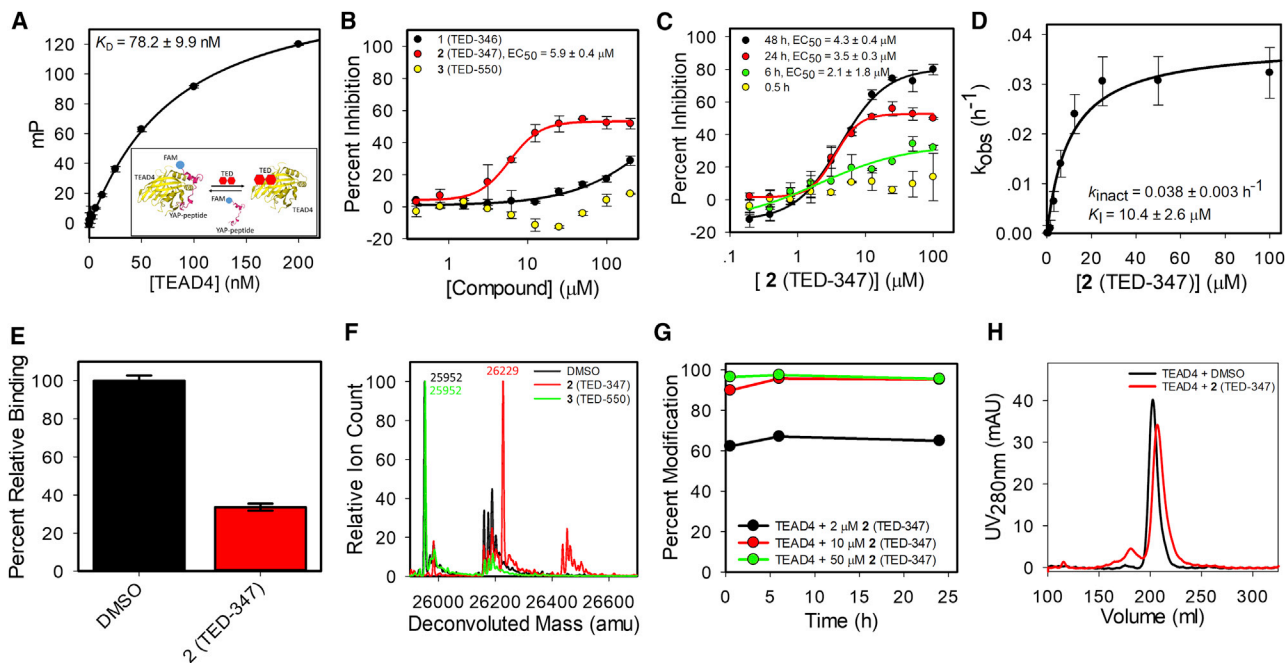


Figure 3. Compounds Inhibit TEAD4·Yap1 Protein-Protein Interaction

(A) Increasing concentration of TEAD4 incubated with 16 nM FAM-labeled Yap (FAM-Yap₆₀₋₉₉) peptide followed by measurements of changes in fluorescence polarization (FP) (mean ± SD, n = 3). Inset: an illustration of the FP assay, where the bound FAM-Yap₆₀₋₉₉ is displaced from TEAD4 due to the interaction by an inhibitor (TED), resulting in loss of polarization.

(B) TEAD4 was incubated with increasing concentration of compounds for 24 hr at 4°C followed by addition of FAM-Yap₆₀₋₉₉ to measure changes in FP (mean ± SD, n = 3).

(C) Time-dependent inhibition of TEAD4 by **2** (TED-347) was assessed by FP using FAM-Yap₆₀₋₉₉ at 10 different concentrations (0.1–100 μM) following 0.5, 6, 24, and 48 hr of incubation at 4°C (mean ± SD, n = 3).

(D) Time-dependent inhibition of TEAD4 by **2** (TED-347) was assessed by FP at 10 concentrations ranging from 0.1 to 100 μM following incubation at 0.5, 6, 24, and 48 hr at 4°C (mean ± SD, n = 3). The observed rate of inactivation (k_{obs}) was calculated at each compound concentration using percent inhibition data at each time point. The rate constant is plotted against the concentration of compound.

(E) TEAD4 was incubated with 50 μM **2** (TED-347) for 24 hr at 4°C, then dialyzed against PBS for 24 hr at 4°C, prior to addition of FAM-Yap₆₀₋₉₉ for FP measurements (mean ± SD, n = 3).

(F) TEAD4 (10 μM) was incubated with 200 μM compounds for 24 hr at 4°C, then analyzed by ESI mass spectrometry.

(G) TEAD4 (10 μM) was incubated with 2, 10, and 50 μM **2** (TED-347) for 0.5, 6, and 25 hr at 4°C and analyzed by ESI mass spectrometry. Percent ratio of the adduct over total protein signal, quantified from the relative ion count, is plotted versus time.

(H) TEAD4 was incubated with DMSO or **2** (TED-347) followed by injection into a SEC column. No significant aggregation was observed.

116.5 ± 5.9 nM (Figure 4D), which was comparable with that of the FAM-YAP₆₀₋₉₉ peptide. As with the peptide FP assay, TEAD4 was incubated with **2** (TED-347) for 24 or 48 hr at 4°C prior to studying its interaction with GST-Yap1 using BLI. As with the FP assay, we observed dose- and time-dependent inhibition of TEAD4 binding to full-length Yap1 (Figure 4E).

Since the palmitate binding pocket and the Cys-367 residue is conserved in all four human TEAD proteins, we tested whether **2** (TED-347) would be active in TEAD2. His-tagged TEAD2 protein was tested in the FP binding assay, where it showed an apparent K_D of 27.6 ± 1.7 nM (Figure 4F). Compounds **1–3** were incubated with TEAD2 for 24 hr at 4°C prior to the addition of the Yap1 peptide, and **2** (TED-347) was shown to inhibit TEAD2, while **1** (TED-346) and **3** (TED-550) were inactive as expected (Figure 4G). We expect that **2** (TED-347) will likely inhibit protein-protein interactions of TEAD1 and TEAD3 with Yap1, considering their close structural similarity to TEAD4.

The selectivity of the compounds was explored with two unrelated protein-protein interactions between (1) the urokinase re-

ceptor (uPAR) and its ligand urokinase (uPA) and (2) the α -subunit of the voltage-gated calcium channel Cav2.2 with its β -subunit Cav β_3 . We have previously developed FP assays for these interactions as we have reported for uPAR (Mani et al., 2013) and Cav β_3 (Chen et al., 2018). Compounds **2** (TED-347) and **3** (TED-550) showed no inhibition of uPAR·uPA or Cav2.2 α · β protein-protein interactions (Figures 4H and 4I). Both proteins have cysteine residues capable of forming covalent bonds. These results further confirm the selectivity of **2** (TED-347).

Structure of **2** in Complex with TEAD2

A TEAD2-**2** complex was formed by soaking TEAD2 crystals with **2** (TED-347). The crystal diffracted to 2.43-Å resolution, and the structure was solved in space group C2 with two TEAD2 per asymmetric unit (Table S2). The overall structure of TEAD2 in complex with **2** (TED-347) is the same as previously published structures, with a $C\alpha$ root-mean-square deviation of 0.59 Å compared with a previously published structure (PDB: 5DQ8). The density of **2** (TED-347) within the central binding pocket is

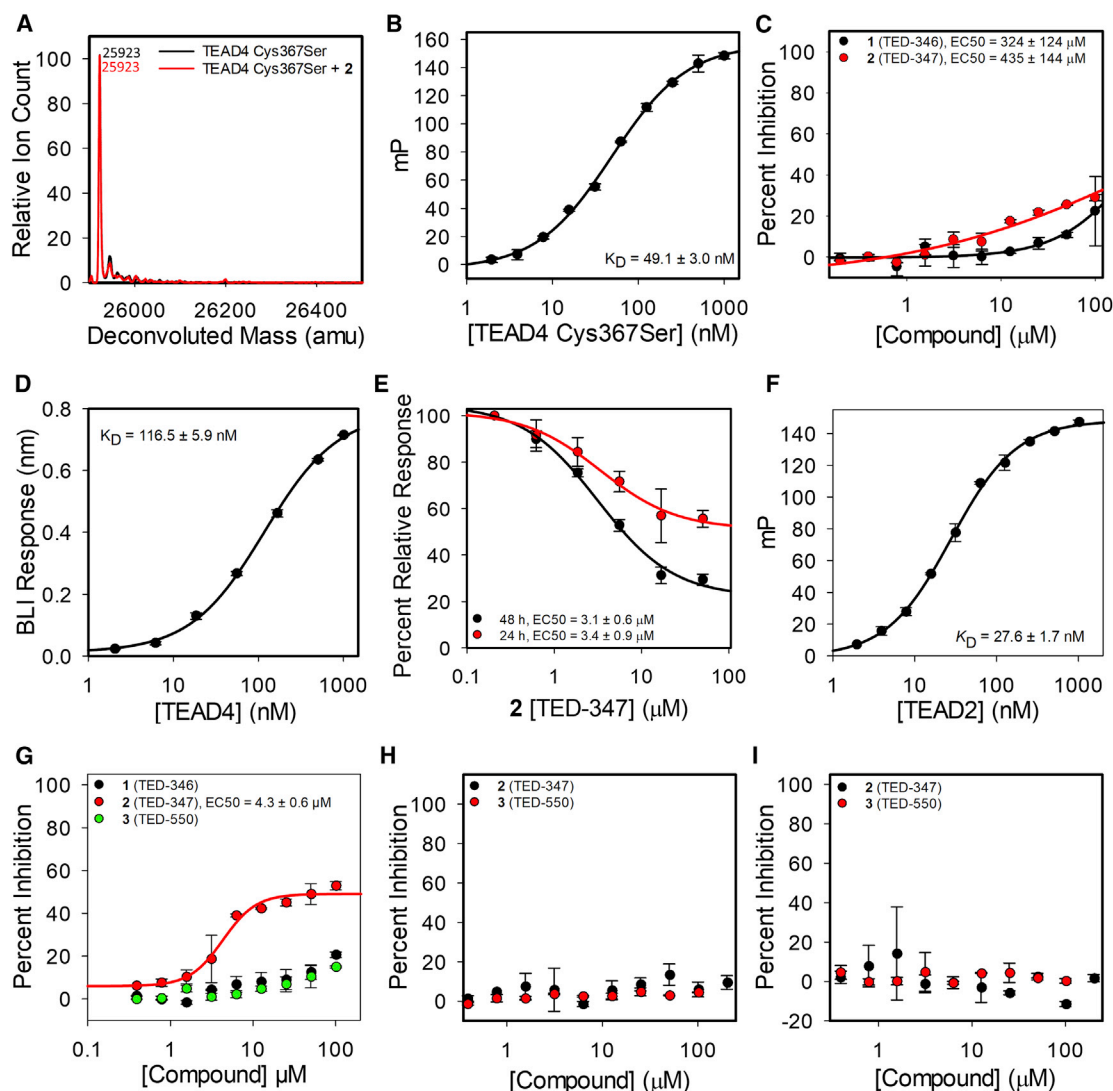


Figure 4. Compound 2 Forms an Adduct at Cys-367 on TEAD4

(A) TEAD4 Cys367Ser mutant (10 μ M) was incubated with 200 μ M compound for 24 hr at 4°C and then analyzed by ESI mass spectrometry.
 (B) Increasing concentration of TEAD4 Cys367Ser mutant was mixed with 16 nM FAM-Yap₆₀₋₉₉ peptide, and FP due to binding was measured (mean \pm SD, n = 3).
 (C) TEAD4 Cys367Ser mutant was incubated with increasing concentration of compounds for 24 hr at 4°C followed by addition of FAM-Yap₆₀₋₉₉ for FP measurements (mean \pm SD, n = 3).
 (D) Biotin-labeled GST-Yap1 was captured onto streptavidin-conjugated biolayer interferometry sensors, which were dipped into varying concentrations of TEAD4. The binding of TEAD4 to the captured Yap was measured by biolayer interferometry (mean \pm SD, n = 3).
 (E) Biotin-labeled GST-Yap1 was captured onto streptavidin-conjugated biolayer interferometry sensors, which were dipped into solutions containing 100 nM TEAD4, pre-incubated with varying concentrations of **2** (TED-347) for 24 or 48 hr at 4°C (mean \pm SD, n = 3).
 (F) Increasing concentration of HIS-TEAD2 was mixed with 16 nM FAM-Yap₆₀₋₉₉ peptide, and FP due to binding was measured (mean \pm SD, n = 3).
 (G) HIS-TEAD2 was incubated with increasing concentration of compounds for 24 hr at 4°C followed by addition of FAM-Yap₆₀₋₉₉ for FP measurements (mean \pm SD, n = 3).
 (H) Urokinase receptor (uPAR) was incubated with varying concentrations of compounds for 24 hr at 4°C followed by addition of a urokinase-derived fluorescently labeled peptide AE147 for FP measurements, according to our previously established protocol (Mani et al., 2013) (mean \pm SD, n = 3).
 (I) The β -3 subunit of the voltage-gated calcium channel Cav2.2 was incubated with varying concentrations of compounds for 24 hr at 4°C followed by addition of an α -subunit peptide that was fluorescently labeled for FP measurement, according to our previously established protocol (Chen et al., 2018) (mean \pm SD, n = 3).

weak (Figure 5A), possibly indicating less than 100% occupancy. To confirm that the observed density is **2** (TED-347) and not palmitate, we soaked out the fatty acid by incubating the crystal in a buffer containing dithiothreitol (DTT) for 2 hr. There is no density within the central pocket after this treatment. We performed

a 3-step soaking experiment, whereby the crystal was first soaked in buffer containing DTT for 2 hr to remove the fatty acid, then exchanged into buffer without DTT for 2 hr, and finally incubated with **2** (TED-347) for 3–4 hr. The crystal quality suffered after the treatment, but an unambiguous positive density

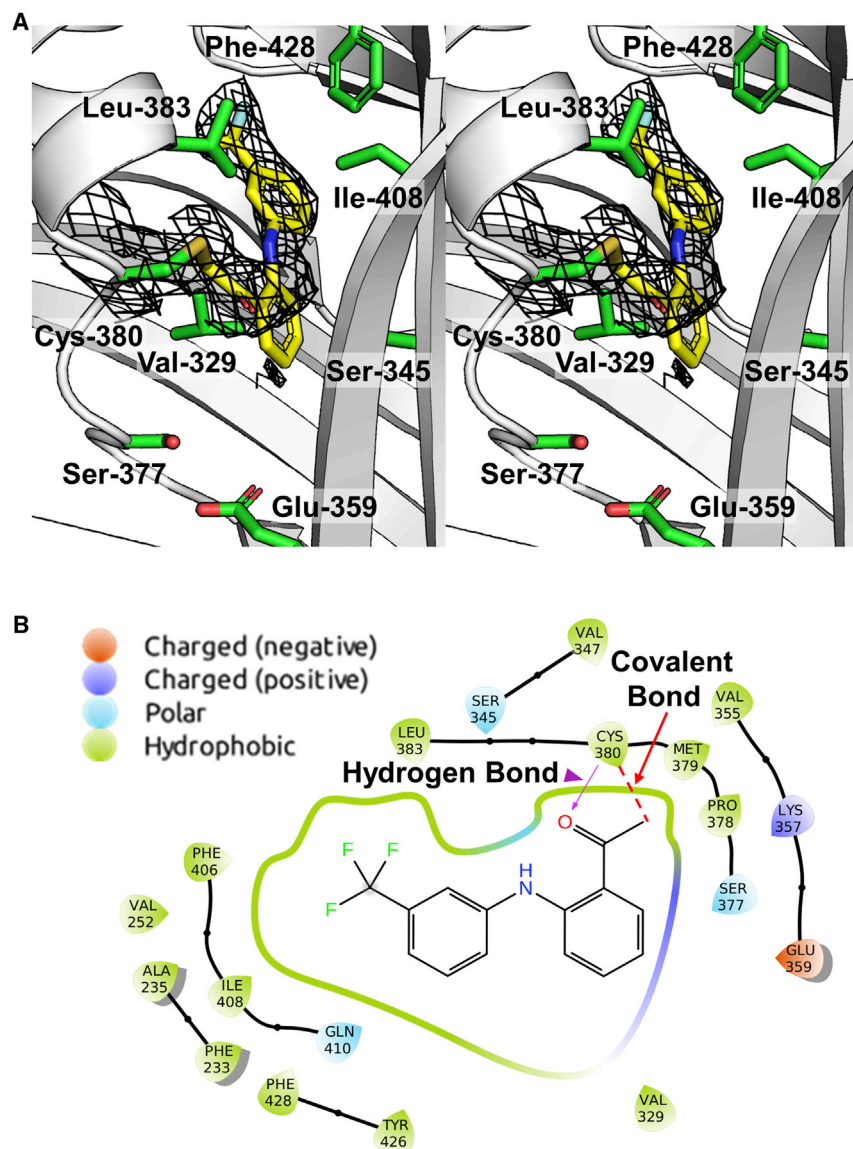


Figure 5. Crystal Structure of TEAD2 in Complex with 2

(A) Stereo image of **2** (TED-347) covalently bound to Cys-380 in the central binding pocket of TEAD2. The $2|Fo| - |Fc|_{\text{calc}}$ map around **2** (TED-347) is illustrated in black mesh. Compound **2** (TED-347) and residues near the reaction site of **2** (TED-347) are shown in sticks (green, carbon; red, oxygen; blue, nitrogen; gold, sulfur) with accompanying labels.

(B) Two-dimensional ligand interaction map of covalently-bound **2** (TED-347) in the central pocket of TEAD2.

the reactivity of the compound, as an electron-withdrawing nitrogen atom was added to the aromatic ring bearing the chloromethyl ketone group. Compound **6** (TED-589) was designed to improve the affinity and selectivity of **2** (TED-347) against TEAD4 by exploiting the nearby pocket. Compounds **7** (TED-587) and **8** (TED-588) were designed to improve the affinity of the compound based on docking studies. After 24 hr of incubation with TEAD4 at 4°C, **4** (TED-548), **5** (TED-551), and **6** (TED-589) showed a maximum inhibition of 31%, 81%, and 51% respectively, while **7** (TED-587) and **8** (TED-588) displayed less than 20% inhibition (Figure S2A). Yet the EC_{50} of compound **4** (TED-548) was substantially lower (nearly an order of magnitude) than its parent **2** (TED-347), as well as the other derivatives. It is worth noting that **5** (TED-551) also inhibited the TEAD4 Cys367Ser mutant, in contrast to **4** (TED-548) and **6** (TED-589) (Figure S2B). Compound **6** (TED-589) had improved EC_{50} of $2.3 \pm 0.8 \mu\text{M}$, while still being selective toward Cys-367. Whole-protein mass spectrometry analysis of TEAD4 with the

was observed in the pocket covalently attached to Cys-380. Compared with the structure of TEAD2 in complex with **1** (PDB: 5DQ8), the first benzene ring of **2** (TED-347) is rotated away from the direction of Val-347 by about 90° to allow the covalent bond to form. The second ring and the trifluoromethyl group is shifted further into the hydrophobic pocket (Figures 5A and 5B). However, due to our multi-step soaking experiment and the resulting positive density, we can visibly see that **2** (TED-347) forms a covalent bond with TEAD2 at our proposed site of Cys-380.

Synthesis and Biochemical Studies of Compound 2 Derivatives

Five derivatives of **2** (TED-347) were synthesized (Figure 2). Compound **4** (TED-548) was designed to more closely mimic palmitate, with an elongated polyethylene glycol-like moiety, which we hypothesized could improve the binding affinity of the compound. Compound **5** (TED-551) was designed to improve

compounds showed that **4** (TED-548), **6** (TED-589), **7** (TED-587), and **8** (TED-588) formed single adducts, consuming all of the protein, while **5** (TED-551) formed more than one covalent complex (Figure S2C). Furthermore, only **5** (TED-551) formed an adduct with the TEAD4 Cys367Ser mutant as evidenced by a minor peak corresponding to a mass of 26,217 (Figure S2D). The lack of TEAD4 inhibition by **7** (TED-587) and **8** (TED-588) (Figure S2A), while still forming 100% adduct with TEAD4 (Figure S2C), again demonstrates that mere binding and reaction to Cys-367 on TEAD4 is not sufficient for inhibition of TEAD4 activity, as demonstrated with iodoacetamide (Figure S1). The five derivatives were also tested for inhibition of TEAD2 binding to Yap1. Compound **5** (TED-551) showed similar inhibition of TEAD2 binding to Yap1, while **4** (TED-548) and **6** (TED-589) were much weaker inhibitors of TEAD2 compared with TEAD4 (Figure S2E).

The three active derivatives showed concentration- and time-dependent inhibition of TEAD4 (Figures S2F–H). The rate of

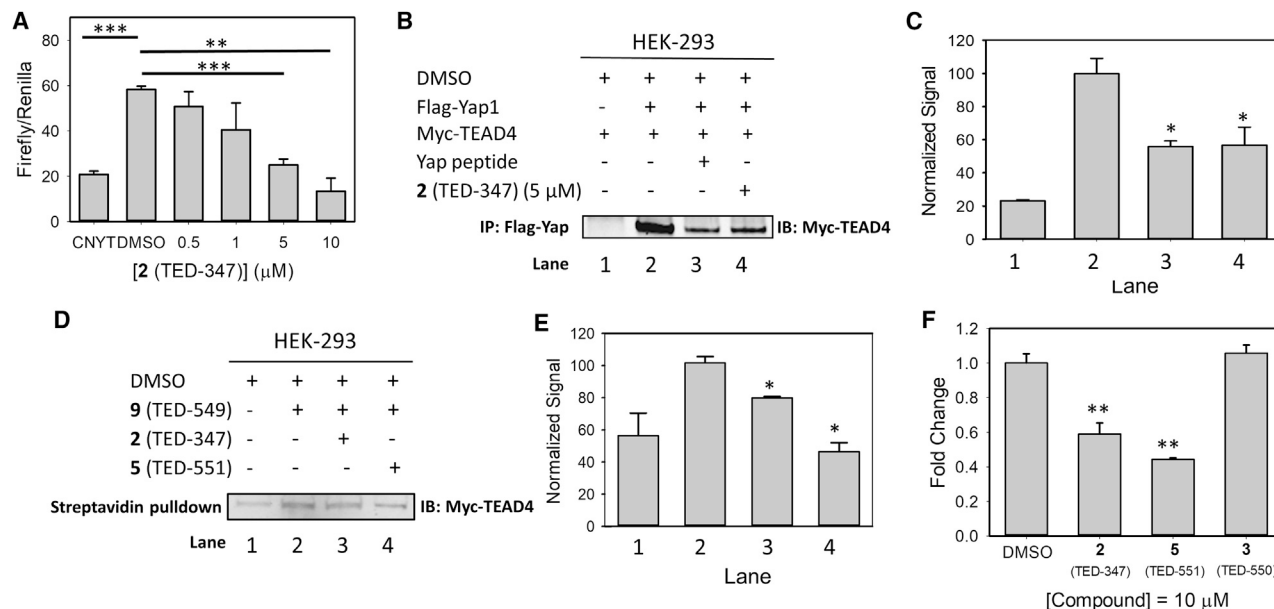


Figure 6. Compound 2 Inhibits TEAD Transcriptional Activity and Protein-Protein Interactions in Cell Culture

(A) The activity of the TEAD4 luciferase reporter was measured in HEK-293 cells treated with either vehicle or compound **2** (TED-347). CNYT corresponds to no transfection; mean \pm SD, $n = 3$ biological replicates.

(B) Co-immunoprecipitation of FLAG-tagged Yap1 and myc-tagged TEAD4 from lysates of HEK-293 cells treated with vehicle, **2** (TED-347), or a peptide (FAM-Yap₆₀₋₉₉) containing the residues in Yap1 that directly bind to TEAD4.

(C) Average normalized values relative to lane A from three biologic replicates; mean \pm SD, $n = 3$ biological replicates.

(D) Lysates from HEK-293 cells treated with **2** (TED-347) or **5** (TED-551) were treated with **9** (TED-549) followed-up by pull-down and detection of TEAD4. Proteins in complexes that were retained by streptavidin pull-down were detected by immunoblot analysis using the indicated antibody.

(E) Average normalized values relative to lane A from three biological replicates; mean \pm SD, $n = 3$ biological replicates.

(F) qRT-PCR analysis of CTGF levels following treatment of HEK-293 cells with compounds for 48 hr; mean \pm SD, $n = 3$ biological replicates. p values were calculated using two-tailed t tests.

* $p < 0.05$, ** $p < 0.005$, *** $p < 0.0005$.

inactivation of **4** (TED-548) is lower than its parent at $0.010 \pm 0.001 \text{ hr}^{-1}$, which resulted in a $t_{1/2}^{\infty}$ of 67.3 hr (Figure S2I). The rate of inactivation of **5** (TED-551) is slightly faster than its parent, with a k_{inact} of $0.049 \pm 0.003 \text{ hr}^{-1}$ corresponding to a half-life of 14.3 hr (Figure S2J). The rate of inactivation of **6** (TED-589), $k_{\text{inact}} = 0.034 \pm 0.003 \text{ hr}^{-1}$ ($t_{1/2}^{\infty} = 20 \text{ hr}$) (Figure S2K), was similar to that of the parent **2** (TED-347).

Small Molecules Inhibit TEAD Transcriptional Activity and Protein Interactions in Cells

The effect of **2** (TED-347) on the intracellular transcriptional activity of TEAD4 was compared with its effects on the interaction of TEAD4 with Yap (Figure 6). Treatment of cells transfected with a TEAD reporter over 48 hr with **2** (TED-347) at 5 μM resulted in over 70% reduction in reporter activity, whereas cells treated with 10 μM of **2** showed a complete loss of reporter activity. Less activity is observed at 24 hr, suggesting time-dependent activity in cells (Figure S3A). To further establish the selectivity of the small molecule, we repeated the TEAD4 transcriptional activity luciferase reporter assays using transfected Cys367Ser mutant. We found that treatment of HEK-293 cells with **2** (TED-347) did not result in the inhibition of TEAD4 transcriptional activity as was observed for wild-type TEAD4 (Figure S3B). Consistent with these effects being a result of disruption of the TEAD4·Yap1 interaction, cells incubated with 5 μM of **2** (TED-347) showed a

significant loss of co-immunoprecipitation of Myc-tagged TEAD4 with FLAG-tagged Yap1 (Figures 6A–6C). To establish that **2** (TED-347) forms a covalent bond with TEAD4 in cells, we synthesized a biotin-conjugated variant, termed **9** (TED-549). Following addition of **9** (TED-549) to cell lysates, TEAD4 was specifically detected by immunoblot analysis in a streptavidin pull-down, consistent with **2** (TED-347) directly engaging TEAD4 in cells in a covalent complex (Figures 6D, 6E, and S3B). The reduction in TEAD4 in **9** (TED-549) containing samples that were also treated with higher concentrations of **2** (TED-347) or **5** (TED-551) indicates that these compounds compete with **9** (TED-549) for binding to TEAD4 (Figures 6D and 6E, lanes 3 and 4). To monitor endogenous TEAD activity, we measured the levels of CTGF transcript (a well-established target of TEAD) by qRT-PCR from control cells and cells incubated with **2** (TED-347) or **5** (TED-551). Cells incubated with compounds **2** (TED-347) and **5** (TED-551) showed a significant reduction in CTGF transcript levels versus control cells (Figure 6F). Cells incubated with compound **3** (TED-550), which lacks the reactive moiety necessary to form an adduct with TEAD4, showed similar levels of CTGF transcript versus control cells.

Compounds Inhibit GBM Cancer Cell Viability

Hippo signaling promotes tumor growth and invasion in a range of cancers including GBM (Artinian et al., 2015; Orr et al., 2011;

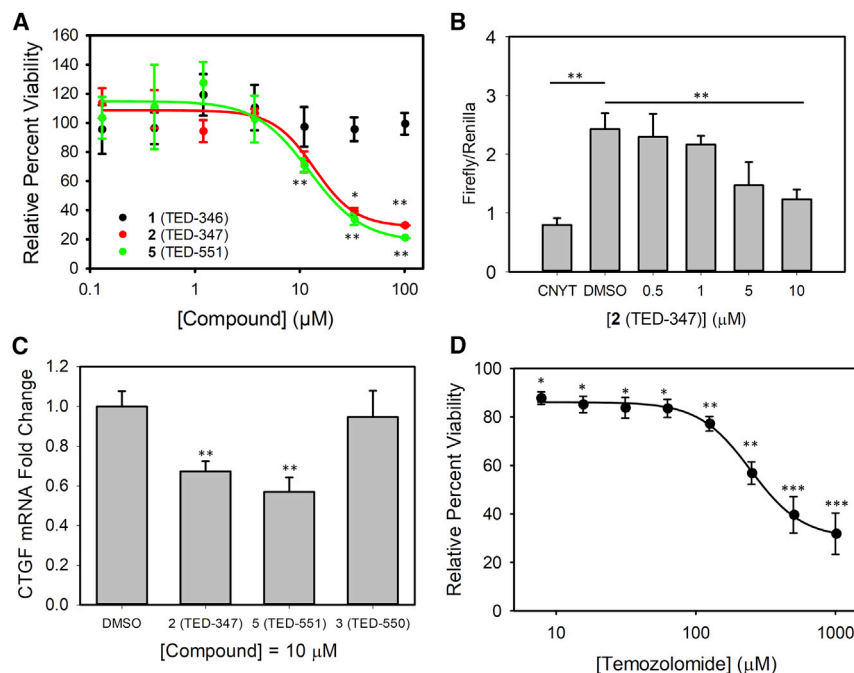


Figure 7. Compound 2 Inhibits Patient-Derived GBM43 Glioblastoma Growth in 3D Spheroids

(A) Spheroids of patient-derived GBM43 glioblastoma cell lines were grown and treated with **1** (TED-346), **2** (TED-347), and **5** (TED-551); mean \pm SD, $n = 3$ biological replicates.

(B) The activity of the TEAD4 luciferase reporter was measured in GBM43 cells treated with either vehicle or compound **2** (TED-347). CNYT corresponds to no transfection; mean \pm SD, $n = 3$ biological replicates.

(C) qRT-PCR analysis of CTGF levels following treatment of GBM43 cells with compounds; mean \pm SD, $n = 3$ biological replicates.

(D) Spheroids of patient-derived GBM43 glioblastoma cell lines were grown and treated with temozolomide; mean \pm SD, $n = 3$ biological replicates. p values were calculated using two-tailed t tests. * $p < 0.05$, ** $p < 0.005$, *** $p < 0.0005$.

Shah et al., 2014). We investigated the effects of **1** (TED-346), **2** (TED-347) and **5** (TED-551) on GBM cell viability using patient-derived GBM43 cells that were grown as three-dimensional spheroids (Figure 7A). Both **2** (TED-347) and **5** (TED-551) inhibited GBM43 cancer cell viability. At 10 μM , which is the concentration used to demonstrate inhibition of TEAD4 activity in cells, the compounds inhibit GBM43 cell viability by 30%. At this concentration, the compound did not show any effect on cell viability of non-transformed normal astrocytes (Figure S4). Compound **1** (TED-346), which does not inhibit TEAD4•Yap1, did not affect GBM43 cancer cell growth (Figure 7A). Compound **2** (TED-347) also inhibited TEAD4 transcriptional activity in GBM43 cells (Figure 7B) in a concentration-dependent manner. Similarly, as shown in Figure 7C, both **2** (TED-347) and **5** (TED-551) suppressed CTGF transcript levels, while **3** (TED-550) had no effect versus cells treated with vehicle. The potency of compounds **2** (TED-347) and **5** (TED-551) were compared with temozolomide, which is the standard of care for patients with glioblastoma. Temozolomide inhibited GBM43 spheroid growth with a substantially higher EC_{50} of $244 \pm 24 \mu\text{M}$ (Figure 7D).

DISCUSSION

The intense interest in Hippo signaling has highlighted the need for small-molecule probes to explore the pathway in normal and pathological processes. However, the development of orthosteric small-molecule inhibitors of the TEAD•Yap interaction has not been successful, likely due to this interaction occurring over a large and featureless binding interface ($1,300 \text{ \AA}^2$) with a K_D in the nanomolar range. While the drug verteporfin was initially proposed to inhibit the TEAD•Yap interaction, it has not been shown to directly bind either TEAD or Yap. Its effects have subsequently been attributed to interactions with other unknown proteins. A crystal structure of TEAD2 bound to flufe-

namic acid (Pobbati et al., 2015) shows that the FDA-approved drug binds to two sites: (1) the palmitate pocket and (2) the TEAD•Yap interface. Flufenamic acid binds weakly to TEAD2 and does not inhibit its interactions, as reported earlier and confirmed in this work.

The three-dimensional structures of TEADs reveal a conserved cysteine (Cys-367) deep within the palmitate binding pocket of TEAD4. Cys-367 spontaneously forms an adduct to palmitoyl-coenzyme A (Chan et al., 2016; Noland et al., 2016), resulting in stability of the TEAD•Yap complex (Mesrouze et al., 2017). Since palmitate does not come in contact with Yap, the process is believed to occur through an allosteric mechanism. This prompted us to postulate that a small molecule that forms a covalent bond with Cys-367 may modulate the TEAD protein-protein interaction with Yap. To test this, we modified flufenamic acid by introducing a reactive chloromethyl ketone moiety and used microsecond explicit-solvent molecular dynamics simulations followed by free energy calculations to investigate the effect of adduct formation on the protein-protein complex. These substantial calculations revealed that non-covalent binding of compounds led to negligible change in the MM-GBSA free energy of the TEAD4•Yap1 complex, whereas covalent bond formation with Cys-367 led to substantial weakening of the interaction. To test this hypothesis we prepared **2** (TED-347), which was found to inhibit the protein-protein interaction in a time-dependent manner. Biochemical studies confirmed that **2** (TED-347) formed a covalent bond with Cys-367 with a $K_i = 10.3 \pm 2.6 \mu\text{M}$ and an inactivation rate constant $k_{\text{inact}} = 0.038 \pm 0.003 \text{ hr}^{-1}$, which corresponds to a half-life $t_{1/2}^{\infty}$ of 18 hr. The compound is selective for TEADs as shown by its ability to inhibit TEAD2 with the same efficacy, while not being able to inhibit unrelated protein-protein interactions, uPAR•uPA and Cav2.2 α • β . Synthesis of several derivatives afforded a structure-activity study and the discovery of three compounds that exhibited: higher affinity but poorer rate of inactivation (compound **4**), better inhibition rate and similar affinity (compound **5**), and higher affinity while maintaining a similar rate of inactivation (compound **6**). In each case, covalent modification of Cys-367 led

to inhibition of the TEAD4·Yap1 protein-protein interaction. Whole-protein mass spectrometry revealed that adduct formation of TEAD4 with **2** (TED-347) was complete within a few minutes, in contrast to the hours required to inhibit the TEAD4·Yap1 protein-protein interaction. The covalent bond formation is therefore not the event that leads to inhibition of the protein-protein interaction. This is further confirmed by studies with iodoacetamide as well as compounds **7** and **8**, all of which readily form adducts to TEAD4 but do not inhibit its interaction with Yap1. Covalent bond formation likely leads to local conformational changes, followed by large-scale conformational and dynamical changes that favor TEAD4 conformational states not suitable for complex formation with Yap1. Comparison of the three-dimensional structure of the non-covalent and covalent complex of **2** (TED-347) with TEAD4 shows that the benzene ring bearing the reactive warhead adopts a different conformation in the covalent complex. This structure may shift the conformation of TEAD4 that leads to inhibition of the TEAD4·Yap1 complex.

Compound **2** (TED-347) was then shown to functionally disrupt the TEAD·Yap1 interaction in cells and to reduce the viability of patient-derived glioblastoma cell lines. Previous studies have shown that Hippo plays a major role in promoting GBM growth and invasion (Artinian et al., 2015; Orr et al., 2011; Shah et al., 2014). HEK-293 and low-passage patient-derived GBM43 cells treated with **2** (TED-347) were found to have reduced TEAD4 transcriptional activity and to lack protein-protein complexes between TEAD4 and Yap1. Pull-down studies confirmed that **2** (TED-347) binds and forms covalent bonds with TEAD4 in these cells. Studies showing GBM43 cells treated with **2** (TED-347) and **5** (TED-551) had significantly reduced rates of proliferation, suggesting that our method to allosterically target the TEAD4·Yap1 interaction is a promising paradigm for the development of therapeutics to treat GBM tumor growth *in vivo*. In fact, these compounds may also be effective against other tumors, as studies have shown several components of the Hippo pathway to act as oncogenes in pancreatic ductal adenocarcinoma and breast cancer.

In sum, the development of **2** (TED-347) and derivatives is a significant breakthrough as there are no existing inhibitors of the TEAD4·Yap1 interaction to enable exploration of Hippo in cell culture and *in vivo*. Furthermore, these compounds suggest that pockets outside tight and challenging protein-protein interaction interfaces with nucleophilic residues may be suitable for the development of allosteric small-molecule inhibitors.

SIGNIFICANCE

The Hippo pathway controls tissue homeostasis and organ size. Hippo signaling leads to phosphorylation of the transcriptional co-activator Yap, which is sequestered in the cytoplasm and degraded. In cancer, Yap phosphorylation is inhibited, resulting in its entry into the nucleus and binding to TEAD transcription factors. TEAD activation leads to the expression of a range of proteins that results in cell growth, apoptotic avoidance, and stem cell self-renewal. Here, we report small-molecule inhibitors of the TEAD·Yap protein-protein interaction following an innovative strategy that consisted of developing a compound that forms a covalent bond

with a conserved cysteine within the palmitate binding pocket of TEADs. This compound led to allosteric inhibition of the TEAD·Yap interaction. Considering the profound interest in Hippo, these compounds will serve as tools to explore the role of Hippo in normal and pathological processes.

STAR★METHODS

Detailed methods are provided in the online version of this paper and include the following:

- KEY RESOURCES TABLE
- CONTACT FOR REAGENT AND RESOURCE SHARING
- EXPERIMENTAL MODEL AND SUBJECT DETAILS
- METHOD DETAILS
 - Luciferase Reporter Assay
 - Covalent Pull Down of TEAD4
 - Co-immunoprecipitation
 - RNA Extraction and Real-Time PCR
 - Sphere-Forming Assay
 - Protein Expression and Purification
 - Size-Exclusion Chromatography
 - Fluorescence Polarization
 - Crystallization of TEAD2 and Structure Refinement
 - Protein Mass Spectrometry
 - Biolayer Interferometry
 - In Silico Protein Preparation
 - Covalent Docking
 - Molecular Dynamics Simulations
 - Free Energy Calculations
 - Synthesis
- QUANTIFICATION AND STATISTICAL ANALYSIS
- DATA AND SOFTWARE AVAILABILITY
- ADDITIONAL RESOURCES

SUPPLEMENTAL INFORMATION

Supplemental Information includes four figures and two tables and can be found with this article online at <https://doi.org/10.1016/j.chembiol.2018.11.010>.

ACKNOWLEDGMENTS

The research was supported by the American Cancer Society Research Scholar grant RSG-12-092-01-CDD (S.O.M.), by an Indiana Drug Discovery Alliance grant (S.O.M.), and by a Vera Bradley Foundation grant (K.B.-E.). Computer time on the Big Red II, Karst, and Carbonate supercomputers at Indiana University is supported in part by Lilly Endowment, through its support for the Indiana University Pervasive Technology Institute, and in part by the Indiana METACyt Initiative. We thank Dr. Jed Fisher for reading the manuscript and for helpful discussions.

AUTHOR CONTRIBUTIONS

K.B.-E., D.Z., G.G.-G., M.K.G., Y.S., D.X., H.E.S., B.J.B., and S.O.M. performed experiments. K.B.-E. and S.O.M. designed experiments and analyzed data. K.E.P. and C.D.W. contributed reagents. K.B.-E., C.D.W., T.W.C., and S.O.M. wrote the paper.

DECLARATION OF INTERESTS

The authors declare no competing interests.

Received: April 29, 2018
Revised: August 27, 2018
Accepted: November 15, 2018
Published: December 20, 2018

REFERENCES

- Adams, P.D., Afonine, P.V., Bunkoczi, G., Chen, V.B., Davis, I.W., Echols, N., Headd, J.J., Hung, L.-W., Kapral, G.J., Grosse-Kunstleve, R.W., McCoy, A.J., Moriarty, N.W., Oeffner, R., Read, R.J., Richardson, D.C., Richardson, J.S., Terwilliger, T.C., and Zwart, P.W. (2010). PHENIX: a comprehensive Python-based system for macromolecular structure solution. *Acta Crystallogr. D. Biol. Crystallogr.* *D66*, 213–221.
- Anbanandam, A., Albarado, D.C., Nguyen, C.T., Halder, G., Gao, X., and Veeraraghavan, S. (2006). Insights into transcription enhancer factor 1 (TEF-1) activity from the solution structure of the TEA domain. *Proc. Natl. Acad. Sci. U S A* *103*, 17225–17230.
- Aragona, M., Panciera, T., Manfrin, A., Giullitti, S., Michielin, F., Elvassore, N., Dupont, S., and Piccolo, S. (2013). A mechanical checkpoint controls multicellular growth through YAP/TAZ regulation by actin-processing factors. *Cell* *154*, 1047–1059.
- Artinian, N., Cloninger, C., Holmes, B., Benavides-Serrato, A., Bashir, T., and Gera, J. (2015). Phosphorylation of the Hippo pathway component AMOTL2 by the mTORC2 kinase promotes YAP signaling, resulting in enhanced glioblastoma growth and invasiveness. *J. Biol. Chem.* *290*, 19387–19401.
- Banks, J.L., Beard, H.S., Cao, Y., Cho, A.E., Damm, W., Farid, R., Felts, A.K., Halgren, T.A., Mainz, D.T., Maple, J.R., et al. (2005). Integrated modeling program, applied chemical theory (IMPACT). *J. Comput. Chem.* *26*, 1752–1780.
- Bayly, C.I., Cieplak, P., Cornell, W.D., and Kollman, P.A. (2013). A well-behaved electrostatic potential based method using charge restraints for deriving atomic charges: the RESP model. *J. Phys. Chem.* *97*, 10269–10280.
- Brooks, B., and Karplus, M. (1983). Harmonic dynamics of proteins: normal modes and fluctuations in bovine pancreatic trypsin inhibitor. *Proc. Natl. Acad. Sci. U S A* *80*, 6571–6575.
- Case, D.A., Babin, V., Berryman, J.T., Betz, R.M., Cai, Q., Cerutti, D.S., Cheatham, T.E., I.I.I., Darden, T.A., Duke, R.E., Gohlke, H., et al. (2014). AMBER14 (San Francisco: University of California).
- Chan, P., Han, X., Zheng, B., DeRan, M., Yu, J., Jarugumilli, G.K., Deng, H., Pan, D., Luo, X., and Wu, X. (2016). Autopalmitoylation of TEAD proteins regulates transcriptional output of the Hippo pathway. *Nat. Chem. Biol.* *12*, 282–289.
- Chen, L., Chan, S.W., Zhang, X., Walsh, M., Lim, C.J., Hong, W., and Song, H. (2010). Structural basis of YAP recognition by TEAD4 in the hippo pathway. *Genes Dev.* *24*, 290–300.
- Chen, X., Liu, D., Zhou, D., Si, Y., Xu, D., Stamatkin, C.W., Ghozayel, M.K., Ripsch, M.S., Obukhov, A.G., White, F.A., and Meroueh, S.O. (2018). Small-molecule $Ca_v\alpha_1$ - $Ca_v\beta$ antagonist suppresses neuronal voltage-gated calcium-channel trafficking. *Proc. Natl. Acad. Sci. U.S.A.* *115*, E10566–10575.
- Darden, T., York, D., and Pedersen, L. (1993). Particle mesh Ewald: an $N \cdot \log(N)$ method for Ewald sums in large systems. *J. Chem. Phys.* *98*, 10089–10092.
- Donohue, E., Balgi, A.D., Komatsu, M., and Roberge, M. (2014). Induction of covalently crosslinked p62 oligomers with reduced binding to polyubiquitinated proteins by the autophagy inhibitor verteporfin. *PLoS One* *9*, e114964.
- Donohue, E., Thomas, A., Maurer, N., Manisali, I., Zeisser-Labouebe, M., Zisman, N., Anderson, H.J., Ng, S.S., Webb, M., Bally, M., et al. (2013). The autophagy inhibitor verteporfin moderately enhances the antitumor activity of gemcitabine in a pancreatic ductal adenocarcinoma model. *J. Cancer* *4*, 585–596.
- Donohue, E., Tovey, A., Vogl, A.W., Arns, S., Sternberg, E., Young, R.N., and Roberge, M. (2011). Inhibition of autophagosome formation by the benzopyrpyrin derivative verteporfin. *J. Biol. Chem.* *286*, 7290–7300.
- Eldridge, M.D., Murray, C.W., Auton, T.R., Paolini, G.V., and Mee, R.P. (1997). Empirical scoring functions: I. The development of a fast empirical scoring function to estimate the binding affinity of ligands in receptor complexes. *J. Comput. Aided Mol. Des.* *11*, 425–445.
- Emsley, P., Lohkamp, B., Scott, W.G., and Cowtan, K. (2010). Features and development of Coot. *Acta Crystallogr. D. Biol. Crystallogr.* *D66*, 486–501.
- Fan, R., Kim, N.G., and Gumbiner, B.M. (2013). Regulation of Hippo pathway by mitogenic growth factors via phosphoinositide 3-kinase and phosphoinositide-dependent kinase-1. *Proc. Natl. Acad. Sci. U S A* *110*, 2569–2574.
- Feig, M., Onufriev, A., Lee, M.S., Im, W., Case, D.A., and Brooks, C.L., 3rd (2004). Performance comparison of generalized born and Poisson methods in the calculation of electrostatic solvation energies for protein structures. *J. Comput. Chem.* *25*, 265–284.
- Fitamant, J., Kottakis, F., Benhamouche, S., Tian, H.S., Chuvin, N., Parachoniak, C.A., Nagle, J.M., Perera, R.M., Lapouge, M., and Deshpande, V. (2015). YAP inhibition restores hepatocyte differentiation in advanced HCC, leading to tumor regression. *Cell Rep.* *10*, 1692–1707.
- Fridell, Y.W.C., Jin, Y., Quilliam, L.A., Burchert, A., McCloskey, P., Spizz, G., Varnum, B., Der, C., and Liu, E.T. (1996). Differential activation of the Ras/extracellular-signal-regulated protein kinase pathway is responsible for the biological consequences induced by the Axl receptor tyrosine kinase. *Mol. Cell. Biol.* *16*, 135–145.
- Frisch, M.J., Trucks, G.W., Schlegel, H.B., Scuseria, G.E., Robb, M.A., Cheeseman, J.R., Scalmani, G., Barone, V., Mennucci, B., Petersson, G.A., et al. (2009). Gaussian 09, Revision D.01 (Gaussian Inc.).
- Greenwood, J.R., Calkins, D., Sullivan, A.P., and Shelley, J.C. (2010). Towards the comprehensive, rapid, and accurate prediction of the favorable tautomeric states of drug-like molecules in aqueous solution. *J. Comput. Aided Mol. Des.* *24*, 591–604.
- Hong, W., and Guan, K.L. (2012). The YAP and TAZ transcription co-activators: key downstream effectors of the mammalian Hippo pathway. *Semin. Cell Dev. Biol.* *23*, 785–793.
- Jacobson, M.P., Pincus, D.L., Rapp, C.S., Day, T.J., Honig, B., Shaw, D.E., and Friesner, R.A. (2004). A hierarchical approach to all-atom protein loop prediction. *Proteins* *55*, 351–367.
- Jiao, S., Wang, H., Shi, Z., Dong, A., Zhang, W., Song, X., He, F., Wang, Y., Zhang, Z., Wang, W., et al. (2014). A peptide mimicking VGLL4 function acts as a YAP antagonist therapy against gastric cancer. *Cancer Cell* *25*, 166–180.
- Jorgensen, W.L., Chandrasekhar, J., Madura, J.D., Impey, R.W., and Klein, M.L. (1983). Comparison of simple potential functions for simulating liquid water. *J. Chem. Phys.* *79*, 926–935.
- Kabsch, W. (2010). XDS. *Acta Crystallogr. D. Biol. Crystallogr.* *D66*, 125–132.
- Li, Z., Zhao, B., Wang, P., Chen, F., Dong, Z., Yang, H., Guan, K.-L., and Xu, Y. (2010). Structural insights into the YAP and TEAD complex. *Genes Dev.* *24*, 235–240.
- Liu-Chittenden, Y., Huang, B., Shim, J.S., Chen, Q., Lee, S.J., Anders, R.A., Liu, J.O., and Pan, D. (2012). Genetic and pharmacological disruption of the TEAD-YAP complex suppresses the oncogenic activity of YAP. *Genes Dev.* *26*, 1300–1305.
- Maier, J.A., Martinez, C., Kasavajhala, K., Wickstrom, L., Hauser, K.E., and Simmerling, C. (2015). ff14SB: improving the accuracy of protein side chain and backbone parameters from ff99SB. *J. Chem. Theory Comput.* *11*, 3696–3713.
- Mani, T., Liu, D., Zhou, D., Li, L., Knabe, W.E., Wang, F., Oh, K., and Meroueh, S.O. (2013). Probing binding and cellular activity of pyrrolidinone and piperidine small molecules targeting the urokinase receptor. *ChemMedChem* *8*, 1963–1977.
- Mauviel, A., Nallet-Staub, F., and Varelas, X. (2012). Integrating developmental signals: a Hippo in the (path)way. *Oncogene* *31*, 1743–1756.
- McCoy, A.J., Grosse-Kunstleve, R.W., Adams, P.D., Winn, M.D., Storoni, L.C., and Read, R.J. (2007). Phaser crystallographic software. *J. Appl. Cryst.* *40*, 658–674.
- McWeeny, R., and Dierksen, G. (1968). Self-consistent perturbation theory. II. extension to open shells. *J. Chem. Phys.* *49*, 4852–4856.
- Mesrouze, Y., Meyerhofer, M., Bokhovchuk, F., Fontana, P., Zimmermann, C., Martin, T., Delaunay, C., Izaac, A., Kallen, J., Schmelzle, T., et al. (2017). Effect

- of the acylation of TEAD4 on its interaction with co-activators YAP and TAZ. *Protein Sci.* **26**, 2399–2409.
- Miller, B.R., 3rd, McGee, T.D., Jr., Swails, J.M., Homeyer, N., Gohlke, H., and Roitberg, A.E. (2012). MMPBSA.py: an efficient program for end-state free energy calculations. *J. Chem. Theory Comput.* **8**, 3314–3321.
- Noland, C.L., Gierke, S., Schnier, P.D., Murray, J., Sandoval, W.N., Sagolla, M., Dey, A., Hannoush, R.N., Fairbrother, W.J., and Cunningham, C.N. (2016). Palmitoylation of TEAD transcription factors is required for their stability and function in hippo pathway signaling. *Structure* **24**, 179–186.
- Olsson, M.H., Sondergaard, C.R., Rostkowski, M., and Jensen, J.H. (2011). PROPKA3: consistent treatment of internal and surface residues in empirical pKa predictions. *J. Chem. Theory Comput.* **7**, 525–537.
- Onufriev, A., Bashford, D., and Case, D.A. (2004). Exploring protein native states and large-scale conformational changes with a modified generalized born model. *Proteins* **55**, 383–394.
- Orr, B.A., Bai, H., Odia, Y., Jain, D., Anders, R.A., and Eberhart, C.G. (2011). Yes-associated protein 1 is widely expressed in human brain tumors and promotes glioblastoma growth. *J. Neuropathol. Exp. Neurol.* **70**, 568–577.
- Petersson, G.A., Bennett, A., Tensfeldt, T.G., Al-Laham, M.A., Shirley, W.A., and Mantzaris, J. (1988). A complete basis set model chemistry. I. The total energies of closed-shell atoms and hydrides of the first-row elements. *J. Chem. Phys.* **89**, 2193–2218.
- Piccolo, S., Cordenonsi, M., and Dupont, S. (2013). Molecular pathways: YAP and TAZ take center stage in organ growth and tumorigenesis. *Clin. Cancer Res.* **19**, 4925–4930.
- Pobbati, A.V., Chan, S.W., Lee, I., Song, H., and Hong, W. (2012). Structural and functional similarity between the Vgll1-TEAD and the YAP-TEAD complexes. *Structure* **20**, 1135–1140.
- Pobbati, A.V., Han, X., Hung, A.W., Weiguang, S., Huda, N., Chen, G.Y., Kang, C., Chia, C.S., Luo, X., Hong, W., et al. (2015). Targeting the central pocket in human transcription factor TEAD as a potential cancer therapeutic strategy. *Structure* **23**, 2076–2086.
- Pobbati, A.V., and Hong, W. (2013). Emerging roles of TEAD transcription factors and its coactivators in cancers. *Cancer Biol. Ther.* **14**, 390–398.
- Pople, J.A., and Nesbet, R.K. (1954). Self-consistent orbitals for radicals. *J. Chem. Phys.* **22**, 571–572.
- Reddy, B.V., and Irvine, K.D. (2013). Regulation of Hippo signaling by EGFR-MAPK signaling through Ajuba family proteins. *Dev. Cell* **24**, 459–471.
- Roe, D.R., and Cheatham, T.E., 3rd (2013). PTRAJ and CPPTRAJ: software for processing and analysis of molecular dynamics trajectory data. *J. Chem. Theory Comput.* **9**, 3084–3095.
- Rosell, R., Bivona, T.G., and Karachaliou, N. (2013). Genetics and biomarkers in personalisation of lung cancer treatment. *Lancet* **382**, 720–731.
- Ryckaert, J.P., Ciccotti, G., and Berendsen, J.J.C. (1977). Numerical integration of the cartesian equations of motion of a system with constraints: molecular dynamics of n-alkanes. *J. Comput. Phys.* **23**, 327–341.
- Sastry, G.M., Adzhigirey, M., Day, T., Annabhimoju, R., and Sherman, W. (2013). Protein and ligand preparation: parameters, protocols, and influence on virtual screening enrichments. *J. Comput. Aided Mol. Des.* **27**, 221–234.
- Schrödinger LLC. (2015). The PyMOL Molecular Graphics System, Version 1.8 (Schrödinger LLC).
- Shah, S.R., Tippens, N.D., Park, J., Mohyeldin, A., Vela, G., Levchenko, A., and Quinones-Hinojosa, A. (2014). Cs-31a novel yap-driven migration and invasion signaling pathway predicts poor outcome in glioblastoma. *Neuro Oncol.* **16** (Suppl 5), v57–v58.
- Shelley, J.C., Cholleti, A., Frye, L.L., Greenwood, J.R., Timlin, M.R., and Uchimaya, M. (2007). Epik: a software program for pKa prediction and protonation state generation for drug-like molecules. *J. Comput. Aided Mol. Des.* **21**, 681–691.
- Still, W.C., Tempczyk, A., Hawley, R.C., and Hendrickson, T. (1990). Semianalytical treatment of solvation for molecular mechanics and dynamics. *J. Am. Chem. Soc.* **112**, 6127–6129.
- Toledo Warshaviak, D., Golan, G., Borrelli, K.W., Zhu, K., and Kalid, O. (2014). Structure-based virtual screening approach for discovery of covalently bound ligands. *J. Chem. Inf. Model.* **54**, 1941–1950.
- Wang, J., Wolf, R.M., Caldwell, J.W., Kollman, P.A., and Case, D.A. (2004). Development and testing of a general amber force field. *J. Comput. Chem.* **25**, 1157–1174.
- Wu, S., Huang, J., Dong, J., and Pan, D. (2003). Hippo encodes a Ste-20 family protein kinase that restricts cell proliferation and promotes apoptosis in conjunction with salvador and warts. *Cell* **114**, 445–456.
- Yu, F.X., and Guan, K.L. (2013). The Hippo pathway: regulators and regulations. *Genes Dev.* **27**, 355–371.
- Yu, F.X., Zhao, B., Panupinthu, N., Jewell, J.L., Lian, I., Wang, L.H., Zhao, J., Yuan, H., Tumaneng, K., Li, H., et al. (2012). Regulation of the Hippo-YAP pathway by G-protein-coupled receptor signaling. *Cell* **150**, 780–791.
- Zhang, W., Gao, Y., Li, P., Shi, Z., Guo, T., Li, F., Han, X., Feng, Y., Zheng, C., Wang, Z., et al. (2014). VGLL4 functions as a new tumor suppressor in lung cancer by negatively regulating the YAP-TEAD transcriptional complex. *Cell Res.* **24**, 331–343.
- Zhao, B., Ye, X., Yu, J., Li, L., Li, W., Li, S., Yu, J., Lin, J.D., Wang, C.Y., Chinnaiyan, A.M., et al. (2008). TEAD mediates YAP-dependent gene induction and growth control. *Genes Dev.* **22**, 1962–1971.
- Zhou, Z., Hu, T., Xu, Z., Lin, Z., Zhang, Z., Feng, T., Zhu, L., Rong, Y., Shen, H., Luk, J.M., et al. (2015). Targeting Hippo pathway by specific interruption of YAP-TEAD interaction using cyclic YAP-like peptides. *FASEB J.* **29**, 724–732.

STAR★METHODS

KEY RESOURCES TABLE

REAGENT or RESOURCE	SOURCE	IDENTIFIER
Antibodies		
Monoclonal Anti-c-Myc antibody produced in mouse	Fisher	Cat# MA1980; RRID: AB_558470
Bacterial and Virus Strains		
E. coli BL-21 (DE3)	New England Biolabs	Cat# C2527H
Chemicals, Peptides, and Recombinant Proteins		
HRV-3C protease	ThermoFisher	Cat# 88946
Thrombin Sepharose Beads	BioVision	Cat# 7925
FAM-Yap(60-99) peptide: FAM- DSETDLEALFNAVM NPKTANVPQTVPMCLRKLPASFCKPP	Synthesized by American Peptide	N/A
Recombinant Protein: GST-TEAD4 (aa 217-434; ref# NP_003204.3)	This study	N/A
Recombinant Protein: GST-TEAD4 C367S (217-434)	This study	N/A
Recombinant Protein: GST-YAP1 (ref# NP_001123617.1)	This study	N/A
Recombinant Protein: HIS-TEAD2 (aa 217-447; ref# NP_003589.1)	This study	N/A
Fetal Bovine Serum- Premium	Atlanta Biologicals	Cat# S11150
DMEM (Dulbecco's Modified Eagle Medium), high glucose	Gibco	Cat# 11965-092
DMEM/F12 1:1	Gibco	Cat# 11320-033
B-27™ Supplement (50X), minus vitamin A	Gibco	Cat# 12587-010
Animal-Free Recombinant Human EGF	Peptotech	Cat# AF-100-15
Animal-Free Recombinant Human FGF-basic	Peptotech	Cat# AF-100-18B
alamarBlue™ Cell Viability Reagent	Invitrogen	Cat# DAL1100
DNA fingerprint analysis	IDEXX BioResearch	N/A
Critical Commercial Assays		
Dual-Glo Luciferase Assay System	Promega	Cat# E2920
GenJet Plus DNA In Vitro Transfection Reagent	SignaGen	Cat# SL100499
Deposited Data		
Crystal structure of human TEAD2-Yap binding domain covalently bound to 2	This paper	PDB: 6E5G
Crystal structure of the palmitoylated human TEAD2 transcription factor	Noland et al., 2016	PDB: 5EMV
Structural basis of YAP recognition by TEAD4 in the Hippo pathway	Chen et al., 2010	PDB: 3JUA
Crystal structure of human transcription factor TEAD2 in complex with palmitate	Chan et al., 2016.	PDB: 5HGU
Crystal structure of human transcription factor TEAD2 in complex with flufenamic acid	Pobbati et al., 2015	PDB: 5DQ8
Experimental Models: Cell Lines		
HEK-293	ATCC	Cat# CRL-1573; sex of cell line is not available.
GBM43	Mayo Clinic	Gift from Dr. Jann Sarkaria; cells were obtained from male patient.
Oligonucleotides		
CTGF Forward Primer-5'TTGCCCCAGACCCAACTA3'	This study	N/A
CTGF Reverse Primer- 5'GCAGGAGGCGTTGTCATT3'	This study	N/A
β-actin Forward Primer-5'TTGCAATGAGCGGTTCC3'	This study	N/A
β-actin Reverse Primer-5'GTTGAAGGTAGTTTCGTGGATG3'	This study	N/A

(Continued on next page)

Continued

REAGENT or RESOURCE	SOURCE	IDENTIFIER
Recombinant DNA		
Plasmid: pGEX-6P-1 TEAD4 (217-434)	This study	N/A
Plasmid: pGEX-6P-1 TEAD4 (217-434) C367S	This study	N/A
Plasmid: pGEX-6P-1 Yap1	This study	N/A
Plasmid: pET-28a TEAD2 (217-447)	This study	N/A
Software and Algorithms		
XDS	Kabsch (2010)	http://xds.mpimf-heidelberg.mpg.de/ ; RRID: SCR_015652
PHENIX	Adams et al. (2010)	http://www.phenix-online.org/ ; RRID: SCR_014224
PHASER	McCoy et al. (2007)	http://www.phaser.cimr.cam.ac.uk/ ; RRID: SCR_014219
Coot	Emsley et al. (2010)	http://www2.mrc-lmb.cam.ac.uk/Personal/pemsley/coot/ ; RRID: SCR_014222
PyMOL v1.8	PyMOL by Schrödinger	https://pymol.org/ ; RRID: SCR_000305
Small-Molecule Drug Discovery Suite v2017-4	Schrödinger	https://www.schrodinger.com/suites/small-molecule-drug-discovery-suite/ ; RRID: SCR_014879
Amber14 (Serial/GPU)	The Amber Project	http://ambermd.org/AmberMD.php ; RRID: SCR_014230
AmberTools16 (MPI/CPU)	The Amber Project	http://ambermd.org/AmberTools.php ; RRID: SCR_014230
Gaussian 09	Gaussian, Inc	http://gaussian.com/ ; RRID: SCR_014897
SigmaPlot 13.0	Systat Software, Inc	https://systatsoftware.com/products/sigmaplot/ ; RRID: SCR_003210
Other		
GSTrap FF column	GE Life Science	Cat# 17513101
HisTrap FF column	GE Life Science	Cat# 17525501
HiLoad 26/600 Superdex 200 pg SEC column	GE Life Science	Cat# 28989336
Envision Multilabel Plate Reader	PerkinElmer	Cat# 2102
Agilent 6520 Accurate Mass Q-TOF	Agilent	Cat# 6520
Agilent 1200 LC-MS	Agilent	Cat# 1200
OctetRed 384	ForteBio	Cat# RED384
96-well Clear Flat Bottom Ultra-Low Attachment Microplate	Corning	Cat# 3474

CONTACT FOR REAGENT AND RESOURCE SHARING

Further information and requests for resources and reagents should be directed to and will be fulfilled by the Lead Contact, Samy O. Meroueh (smeroueh@iu.edu).

EXPERIMENTAL MODEL AND SUBJECT DETAILS

HEK-293 and GBM43 cells were cultured in DMEM medium with glutamine (Cellgro, Manassas, VA) supplemented with 10% FBS and 1% penicillin/streptomycin in 5% CO₂ at 37°C.

E. coli BL-21 (DE3) strain was purchased from New England Biolabs (Ipswich, MA) and cultured and grown in Luria Broth media at 37°C.

METHOD DETAILS

Luciferase Reporter Assay

HEK-293 or GBM43 cells were plated at 2.4×10^4 cells/well in a 96-well microplate and were transfected after 24 hr with the a pGL3.1 reporter containing the CTGF promoter and a plasmid encoding TK-Renilla luciferase in combination with control vectors or vectors that express Yap1 and TEAD4. After 48 hr, cells were treated with 0.5, 1.0, 5.0 or 10 μ M of **2** (TED-347) for another 48 hr. Luciferase

activity was measured according to the Dual-Glo luciferase assay (Promega) instructions using a Biotek Synergy Neo2 plate reader. Relative luciferase activity represents the ratio of firefly/renilla luminescence values.

Covalent Pull Down of TEAD4

HEK-293 cells transfected with the myc-TEAD4 construct were grown for 48 hr and then treated with DMSO or with 25 μ M of **2** (TED-347) for an additional 48 hr. Cells were then harvested in lysis buffer (50 mM Tris-HCl, pH 7.3, 150 mM NaCl, 0.5 mM EDTA, 1% Triton X-100, PhosSTOP phosphatase inhibitor cocktail, and EDTA-free protease inhibitors cocktail). Cell lysates containing 2 mg of protein were incubated with the indicated compounds or DMSO for 24 hr. Extracts were then incubated with Dynabeads M-280 Streptavidin (Sigma-Aldrich) for 2 hr at 4°C. The Dynabeads were then washed and bound proteins were denatured and eluted according to the manufacturer's instructions. Relative levels of myc-TEAD4 from each complex were measured by immunoblot analysis with the anti-c-Myc antibody (1:5,000, Sigma-Aldrich).

Co-immunoprecipitation

HEK293 cells transfected with Flag-YAP1 alone or in combination with myc-TEAD4 were incubated with DMSO or the indicated amount of compounds for 48 hr. Cells were harvested in lysis buffer (50 mM Tris-HCl, pH 7.3, 150 mM NaCl, 0.5 mM EDTA, 1% Triton X-100, PhosSTOP phosphatase inhibitor cocktail, and complete EDTA-free protease inhibitors cocktail). Extracts were immunoprecipitated with magnetic beads coupled to the M2 (anti-Flag) antibody (Sigma-Aldrich) for 4 hr at 4°C. The Dynabeads were then washed and bound proteins were denatured and eluted according to the manufacturer's instructions. Relative levels of myc-TEAD4 from each complex was then measured by immunoblot analysis with the anti-c-Myc antibody (1:5,000, Sigma-Aldrich).

RNA Extraction and Real-Time PCR

HEK293 cells co-transfected the Flag-YAP and myc-TEAD4 constructs were incubated with DMSO or the indicated amount of compounds for 48 hr. Total RNA was purified using the RNeasy plus mini kit (QIAGEN, Hilden, Germany) according to the manufacturer's instructions. Complementary DNA was synthesized from 500 ng total RNA with Oligo-dT primers and the Multi-Scribe reverse transcriptase (Fisher, Waltham, MA) according to the manufacturer's instructions.

Real-time PCR reactions utilized 100 ng cDNA, 200 nM gene specific primers and the Sensifast No-ROX mix (Bioline, Taunton, MA) in a total volume of 20 μ L. All measurements were carried out in triplicate using an Eppendorf Mastercycler® RealPlex2. The sequences of primers for CTGF were forward, 5'-TTGGCCAGACCCAACTA-3; and reverse, 5'-GCAGGAGGCGTTGCATT-3'. The primer sequences for β -actin were forward, 5'-TTGGCAATGAGCGTTCC-3; and reverse, 5'-GTTGAAGGTAGTTTCGTGGATG-3'.

Sphere-Forming Assay

The GBM43 xenograft tissue was a kind gift from Dr. Jann Sarkaria (Mayo Clinic, Rochester, MN), and tumors were expanded by passage in the flank of NOD/SCID- γ^{null} mice. To generate GBM43 cell lines, tumors were harvested, disaggregated, and maintained in 2.5% FBS for 14 days on Matrigel-coated plates (BD Biosciences) to remove murine fibroblasts. In-vitro GBM43 cell lines were propagated in DMEM with 10% FBS for no more than 7 passages. Cell line identity was confirmed by DNA fingerprint analysis (IDEXX BioResearch) for species and baseline short-tandem repeat analysis testing. GBM43 spheroids were generated by plating early-passage cells at 2.5×10^4 cells per well in 96-well ultralow attachment plates (Corning Inc.) in DMEM/F12 (1:1; GIBCO) supplemented with 2% B27 supplement (GIBCO), 20 ng/mL epidermal growth factor (EGF), and 20 ng/mL fibroblast growth factor (FGF) (Peprotech) for 2 days. The spheroids were then treated with compounds **1** (TED-346), **2** (TED-347) and **5** (TED-551) and growth analyzed by Alamar blue staining.

Protein Expression and Purification

TEAD4 (217-434), TEAD4 (217-434) Cys367Ser mutant, and Yap1 (Full-length) were expressed as GST-fusion proteins in BL-21 (DE3) strain of *E. coli* from the pGEX-6P-1 vector. Transformed bacteria were grown in LB at 37°C until they reached an OD₆₀₀ of 0.6 – 0.8. Isopropyl- β -D-galactoside (IPTG) was added to a final concentration of 0.5 mM and cells were then incubated at 16°C for 16 hr. Cell pellets were re-suspended in a buffer containing 200 mM NaCl, 20 mM Tris, 2 mM dithiothreitol (DTT), pH 8.0, and lysed by passage through a microfluidizer. Cell debris was removed by centrifugation at 35,000 x g for 1 hr. Clarified lysates were loaded onto a pre-equilibrated 5 mL GSTrap HP column at 1 ml/min. The column was washed with 5 column volumes of buffer and the protein was eluted with 10 mM reduced glutathione in the same buffer. The protein was further purified on a HiLoad 26/600 Superdex 200 pg SEC column (GE, Boston, MA) with 100 mM NaCl, 20 mM Tris, 2 mM DTT, pH 8.0 as buffer. The GST-tag was cleaved from proteins by incubation with the HRV-3C protease (ThermoFisher, Waltham, MA) at 100:1 w/w ratio while dialyzing against PBS with 5 mM β -mercaptoethanol for 48 hr at 4°C. The cleavage solution was passed through a GSTrap HP column to remove the cleaved GST and the HRV-3C protease. Cleavage was verified by SDS-PAGE and mass spectrometry.

TEAD2 (217-447) was expressed as N-terminal HIS-fusion protein in BL-21 (DE3) strain of *E. coli* from the pET-28a vector. Transformed bacteria were grown in Terrific Broth at 37°C until they reached an OD₆₀₀ of 0.6 – 0.8. IPTG was added to a final concentration of 0.5 mM and cells were then incubated at 16°C for 16 hr. Cell pellets were re-suspended in a buffer containing 500 mM NaCl, 50 mM HEPES, 8 mM β -mercaptoethanol, pH 7.5 and lysed by multiple passages through a microfluidizer. Cell debris was removed by centrifugation at 35,000 x g for 1 hr. Clarified lysates were loaded onto a pre-equilibrated 5 mL HisTrap FF column at 1 mL/min. The column was washed with 100 mL of buffer containing 300 mM NaCl, 25 mM HEPES, 1 mM TCEP, 5 % v/v glycerol, 30 mM imidazole, pH 7.5 prior to elution with the same buffer containing 300 mM imidazole. The protein was further purified on a HiLoad 26/600

Superdex 200 pg SEC column (GE, Boston, MA) with 150 mM NaCl, 25 mM HEPES, 1 mM TCEP, pH 7.5 as buffer. For crystallization trials, the elute from the HisTrapFF affinity chromatography was dialyzed against 150 mM NaCl, 50 mM Tris pH 8.0 for 2 hr, then cleaved with 1:100 w/w thrombin at 4°C overnight. The cleaved protein was dialyzed against 300 mM NaCl, 25 mM HEPES, 1 mM TCEP, 5 % v/v glycerol, 10 mM imidazole, pH 7.5. The cleaved HIS-tag was removed by passing through the HisTrap FF column. TEAD2 without the HIS-tag was further purified on SEC, as above.

Size-Exclusion Chromatography

2 ml of 6.3 μM GST-TEAD4 in PBS was incubated with 100 μM **2** (TED-347) in 2 % v/v DMSO or DMSO without compound for 24 hr at 4°C. After the incubation, the samples were injected into a HiLoad 26/600 Superdex 200 pg SEC column, pre-equilibrated with PBS. The elution profile of the column was analyzed for protein aggregation.

Fluorescence Polarization

GST-TEAD4, GST-TEAD4 Cys367Ser mutant or HIS-TEAD2 interaction with Yap1 was investigated using a fluorescently-labeled peptide (FAM-Yap₆₀₋₉₉), consisting of FAM-labeled TEAD-binding peptide fragment of Yap1 (FAM-DSETDLEALFNAVMNPK TANVPQTVPMCLRLKPASFCKPP), which has a disulfide bridge (American Peptide, Sunnyvale, CA). Addition of FAM-Yap₆₀₋₉₉ to the TEAD was followed by measurement of changes in polarization. 40 μL of 125 nM GST-TEAD4 WT or GST-TEAD4 Cys367Ser in assay buffer (PBS with 0.01 % v/v Triton-X100) or 40 μL of 64 nM HIS-TEAD2 was added to a 384-well black polystyrene plate (Cat. No. 262260; Nunc, Roskilde, Denmark) and incubated with 5 μL of 2 – 2000 μM serially diluted compounds in assay buffer supplemented with 20 % v/v DMSO for 24 hr at 4°C. Finally, 5 μL of 160 nM FAM-Yap₆₀₋₉₉ peptide was added, the plate centrifuged, and the polarization was measured on an Envision Multilabel Plate Reader (PerkinElmer, Waltham, MA) using a filter set with excitation and emission wavelengths of 485 and 535 nm, respectively. Percent inhibition was calculated as relative to a minimum inhibition control, which is without compound, and a maximum inhibition control, which is without a TEAD.

For the determination of the inhibition efficiency k_{inact}/K_i , the protein – compound incubation time was varied between 0.5 – 48 hr, prior to the addition of the FAM-Yap₆₀₋₉₉ peptide and fluorescence polarization measurements. The progressive decrease in TEAD activities were plotted against time for all 10 concentrations (0.2 – 100 μM) of the compounds and the observed rate of inhibition (k_{obs}) was calculated by fitting a simple exponential function. The observed rate of inhibition was then plotted against the concentration of

the compound and a polynomial function $k_{\text{obs}} = \frac{k_{\text{inact}} [\text{Inhibitor}]}{K_i + [\text{Inhibitor}]}$ was fitted to determine the k_{inact} and K_i values.

Crystallization of TEAD2 and Structure Refinement

Purified TEAD2 was concentrated to ~12 mg/mL and crystallized at 20°C using the hanging-drop vapor-diffusion method with a reservoir solution containing 0.1 M HEPES (pH 7.2 – 7.4) and 2.4 – 2.8 M sodium formate. The crystals were soaked in reservoir solution supplemented with 3 – 5 mM of **2** (TED-347) and 25 % v/v glycerol for 3 hr and were subsequently flash-cooled in liquid nitrogen. To rule out the possibility that the observed density of **2** (TED-347) was not the endogenous S-palmitoylation from protein expression (Noland et al., 2016), some crystals were soaked in a cryo-protectant solution supplemented with 2 mM DTT for 2 hr to soak out the fatty acid. The crystal structure of these crystals was solved and no extra electron-density was observed. Another batch of crystals were soaked in three steps: (1) in a cryo-protectant solution supplemented with 2 mM DTT for 2 hr, (2) in a cryo-protectant solution (wash) for 2 hr, and (3) in a cryo-protectant solution supplemented with 3–5 mM of **2** (TED-347) for 3 hr.

Data was collected at beamline 4.2.2 at the Advanced Light Source (ALS, Berkeley, CA, USA) and processed with XDS. All crystals contained two molecules per asymmetric unit and the symmetry corresponded to space group C2. Molecular Replacement was used to obtain the initial phases using Phaser and the crystal structure of TEAD2 transcriptional activation domain (PDB: 5EMV) as the search model. Initial model building was carried out using Autobuild in PHENIX. The final model (R_{free} 0.268, with good geometry and no Ramachandran outliers) was obtained by iterative cycles of manual building in Coot and refinements with PHENIX-refine.

Protein Mass Spectrometry

Compounds at 200 μM concentrations (unless otherwise specified) were incubated with 10 μM TEAD4 WT or TEAD4 Cys367Ser mutant in 20 mM NH₄OAc for 24 hr (unless otherwise specified) at 4°C. The samples were centrifuged at 20,000 x g for 20 min to remove precipitants prior to being injected into an empty column on an Agilent 1200 liquid chromatography system (Agilent, Santa Clara, CA), using 80 % Buffer A (H₂O, 5 mM NH₄OAc) and 20 % Buffer B (ACN, 5 mM NH₄OAc), and the masses were detected on an Agilent 6520 Accurate Mass Q-TOF.

Biolayer Interferometry

Biolayer Interferometry was measured on OctetRed 384 (ForteBio, Menlo Park, CA) using PBS with 0.025% v/v Tween-20 at 30°C with constant shaking at 1000 rpm. Streptavidin-conjugated sensors (ForteBio, Menlo Park, CA) were loaded with 30 μg/ml biotin-labeled GST-Yap or biocytin and were introduced to 1–1000 nM TEAD4. The sensors were regenerated with 5 mM HCl solution after each interaction. For compound inhibition study, 100 nM TEAD4 was pre-incubated with 0.1 – 100 μM **2** (TED-347) in 2 % v/v DMSO for 24 hr at 4°C prior to interaction with captured GST-Yap.

In Silico Protein Preparation

The crystal structures of TEAD4·YAP (PDB: 3JUA), TEAD2·PLM (PDB: 5HGU, palmitic acid), and TEAD2·FLF (PDB: 5DQ8, flufenamic acid) were retrieved and prepared using the Protein Preparation Wizard in the Schrödinger software package (Schrödinger LLC, New York, NY, 2017) (Greenwood et al., 2010; Sastry et al., 2013). Bond orders were assigned and hydrogen atoms were added. Missing side chains and loops were introduced using the Prime module (Jacobson et al., 2004). The resulting protein and compound structures were protonated at pH 7.0 using PROPKA (Olsson et al., 2011) and Epik (Shelley et al., 2007), respectively. The structure of **2** (TED-347) was generated by replacing the carboxylic acid on FLF with chloromethyl ketone. Subsequently, the binding modes of PLM and **2** (TED-347) to TEAD4 were obtained using the *align* function in PyMOL (Schrödinger, 2015).

Covalent Docking

The covalent structure of TEAD4·**2** was generated using CovDock (Toledo Warshaviak et al., 2014). The chloromethyl ketone group of **2** was defined as the reaction group for a nucleophilic substitution reaction with the TEAD4 Cys-367. Residues within 3.0 Å of **2** were refined during covalent docking. The covalent bond parameters from the OPLS force field (Banks et al., 2005) were extracted.

Molecular Dynamics Simulations

The structures of TEAD4·Yap1, TEAD4·Yap1·PLM, non-covalent [TEAD4·**2**]·Yap1, and covalent [TEAD4·**2**]·Yap1 were used to run molecular dynamics simulations using the AMBER14 software package (Case et al., 2014). The restrained electrostatic potential (RESP) atomic charges (Bayly et al., 2013) of PLM and **2** in the covalent and non-covalent complexes were calculated at the HF/6-31G* level (McWeeny and Diercksen, 1968; Petersson et al., 1988; Pople and Nesbet, 1954) using the Gaussian 09 package (Frisch et al., 2009). In the covalent [TEAD4·**2**]·Yap1 complex, **2**, Leu-366, Cys-367, and Glu-368 were extracted for RESP charge fitting. The atom charges of Cys-367 were replaced by RESP charges and the optimized parameters of bond length, bond angle, and dihedral angle between Cys-367 and **2** were used to build new *frmod* parameters. The α -carbon atom of **2** and sulfur atom of Cys-367 were bonded using *tLeap* program.

Complexes were immersed in a box of TIP3P water molecules (Jorgensen et al., 1983). No atom on the complex was within 14 Å of any side of the box. The solvated box was further neutralized with Na⁺ or Cl⁻ counterions using the *tLeap* program. Simulations were carried out using the GPU accelerated version of the *pmemd* program with ff14SB (Maier et al., 2015) and gaff force fields (Wang et al., 2004) in periodic boundary conditions. All bonds involving hydrogen atoms were constrained by using the SHAKE algorithm (Ryckaert et al., 1977), and a 2 femtoseconds (fs) time step was used in the simulation. The particle mesh Ewald (PME) method (Darden et al., 1993) was used to treat long-range electrostatics. Simulations were run at 298 K under 1 atm in NPT ensemble employing Langevin thermostat and Berendsen barostat. Water molecules were first energy-minimized and equilibrated by running a short simulation with the complex fixed using Cartesian restraints. A series of energy minimizations were subsequently applied in which the Cartesian restraints were gradually relaxed from 500 kcal·Å⁻² to 0 kcal·Å⁻², and the system was subsequently gradually heated to 298 K with a 48 ps molecular dynamics run. For each complex, we generated 50 independent simulations (replicates) that are each 50 ns in length. The initial velocity of each replicate was randomly assigned. In total, 2.5 μs of simulation was run for each complex.

Free Energy Calculations

In each of the 50 trajectories (50 ns in length), the first 2 ns were discarded for equilibration. Snapshots were saved every 1 ps, yielding 48000 structures per trajectory. 30000 snapshots were selected at regular intervals for free energy calculations using the *cpptraj* program (Roë and Cheatham, 2013). The Molecular Mechanics-Generalized Born Surface Area (MM-GBSA) (Still et al., 1990) method was used to calculate the free energy using the *MMPBSA.py* script (Miller et al., 2012). The calculation using the GB method was performed with *sander* and Onufriev's GB model (Feig et al., 2004; Onufriev et al., 2004). Solvent-accessible surface area (SASA) calculations were switched to the icosahedron (ICOSA) method, where surface areas are computed by recursively approximating a sphere around an atom, starting from an icosahedron. Salt concentration was set to 0.1 M. The entropy was estimated by normal mode calculations (Brooks and Karplus, 1983) with the *mmpbsa_py_nabnmode* module by selecting 150 of the 30000 snapshots used in the free energy calculations at regular intervals. The maximum number of cycles of minimization was set to 10000. The convergence criterion for the energy gradient to stop minimization was 0.5. In total, 30000 frames were used for each MM-GBSA calculations while 150 frames were used for each normal mode analysis. All other parameters were left at default values.

The MM-GBSA binding free energy is expressed as:

$$\Delta G_{\text{MM-GBSA}} = \Delta E_{\text{GBTOT}} - T\Delta S_{\text{NMODE}}$$

where ΔE_{GBTOT} is the combined internal and solvation energies, T is the temperature (298.15 K). ΔS_{NMODE} is the entropy estimated by normal mode calculations. The total enthalpy from the generalized Born model, ΔE_{GBTOT} , is the sum of 4 components:

$$\Delta E_{\text{GBTOT}} = \Delta E_{\text{VDW}} + \Delta E_{\text{ELE}} + \Delta E_{\text{GB}} + \Delta E_{\text{SURF}}$$

where ΔE_{VDW} and ΔE_{ELE} are the van der Waals and electrostatic energies, respectively, and ΔE_{GB} and ΔE_{SURF} are the polar and non-polar desolvation energies, respectively. All binding energies are determined by:

$$\Delta E = E^{\text{COM}} - E^{\text{REC}} - E^{\text{LIG}}$$

where E^{COM} , E^{REC} and E^{LIG} are total energies corresponding to the complex, receptor, and ligand, respectively. The relative difference in free energy is determined by:

$$\Delta\Delta G = \Delta G_{COM} - \Delta G_{APO}$$

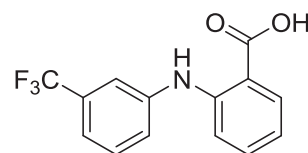
where ΔG_{COM} and ΔG_{APO} are the covalent or non-covalent complex and the unbound native *apo* complex, respectively.

Synthesis

All chemicals were purchased from either Aldrich or Acros and used as received. Column chromatography was carried out with silica gel (25–63 μ). Mass spectra were measured on an Agilent 6520 Accurate Mass Q-TOF instrument. ^1H NMR spectra were recorded in CDCl_3 or Methanol- d_4 on a Bruker 500 MHz spectrometer. Chemical shifts are reported using residual CHCl_3 or MeOH as internal references. All compounds that were evaluated in biological assays had >95% purity by HPLC.

2-((3-(trifluoromethyl)phenyl)amino)benzoic acid (**1**, TED-346)

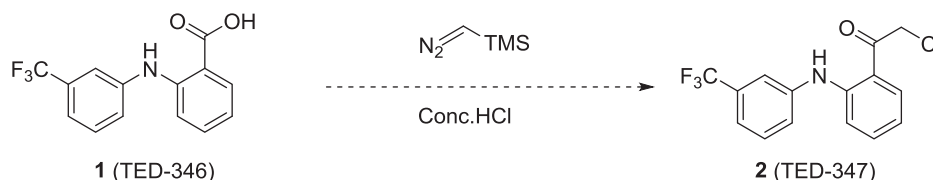
Purchased from a commercial source.



1 (TED-346)

^1H NMR (400 MHz, CDCl_3). δ 9.42 (s, 1H), 8.09–8.07 (dd, $J=8.0\text{Hz}$, $J=1.2\text{Hz}$, 1H), 7.51 (s, 1H), 7.49–7.40 (m, 3H), 7.36–7.34 (m, 1H), 7.27–7.25 (m, 2H), 6.87–6.83 (t, $J=8.0\text{Hz}$, 1H).

Synthesis of 2-chloro-1-(2-((3-(trifluoromethyl)phenyl)amino)phenyl) ethanone (**2**, TED-347)

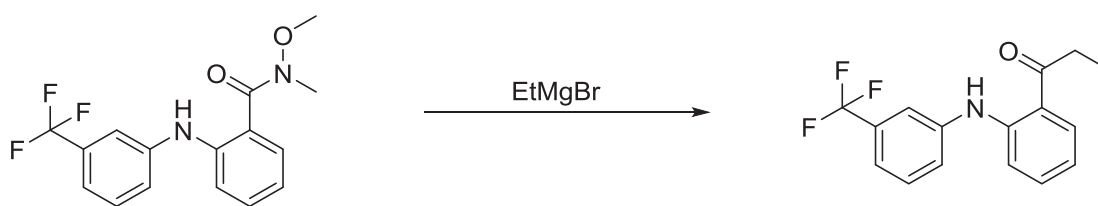


1 (TED-346)

2 (TED-347)

A solution of 2-((3-(trifluoromethyl)phenyl)amino)benzoic acid (**1**, 200 mg, 0.71 mmol) in SOCl_2 (6 mL) was refluxed for 1 hr. The mixture was evaporated to dryness. The residue was dissolved in MeCN (10 mL) and cooled to 0°C , followed by the addition of TMSCHN_2 (1.07 mmol, 0.5 mL). It was stirred for 1 hr, and *conc.* HCl (0.5 mL) was added to the mixture at 0°C . The mixture was stirred for 0.5 hr. The mixture was quenched with NaHCO_3 (aq) and diluted with water. The mixture was extracted with EA (15 mL x 2). The combined organic layers were dried with Na_2SO_4 , filtered and concentrated. The residue was purified by Prep-TLC (PE / EA = 5 / 1) to give 2-chloro-1-(2-((3-(trifluoromethyl)phenyl)amino)phenyl)ethanone (6.4 mg, 2.8%); ^1H NMR (400 MHz, CDCl_3): δ 10.43 (s, 1H), 7.79–7.64 (dd, $J=4.0\text{Hz}$, $J=0.8\text{Hz}$, 1H), 7.51–7.47 (m, 1H), 7.45–7.41 (m, 1H), 7.38–7.36 (m, 3H), 7.29–7.26 (m, 1H), 6.85–6.82 (m, 1H), 4.75 (s, 1H); ^{13}C NMR (400 MHz, CDCl_3) δ 193.41, 147.80, 140.67, 135.66, 132.16, 131.86, 130.04, 125.86, 125.20, 122.49, 120.71, 120.67, 120.63, 119.33, 119.30, 119.26, 117.84, 116.87, 114.65, 46.53. LRMS calculated for $\text{C}_{15}\text{H}_{12}\text{ClF}_3\text{NO}^+$ $[\text{M}+\text{H}]^+$, 314.05 found 314.0.

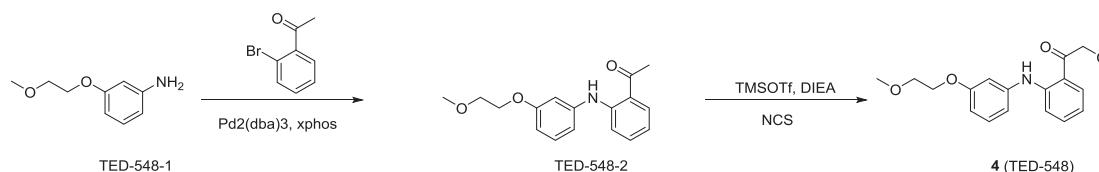
Synthesis of 1-(2-((3-(trifluoromethyl)phenyl)amino)phenyl)propan-1-one (**3**, TED-550)



3 (TED-550)

To a solution of N-methoxy-N-methyl-2-((3-(trifluoromethyl)phenyl)amino)benzamide (100 mg, 0.31 mmol) in THF (5 mL) was added 1 M EtMgBr in THF (1.8 mL) at -78 °C under N₂. The resulting mixture was warmed to rt and stirred for 5 hr. The reaction mixture was quenched with sat. NH₄Cl (20 mL), and extracted with EA (5 mL x 3). The organic phase was washed with brine, dried over Na₂SO₄, and filtered. The filtrate was concentrated. The residue was purified by prep-TLC (PE/EA=20/1) to give 1-(2-((3-(trifluoromethyl)phenyl)amino)phenyl)propan-1-one (15 mg, 16.5%); ¹H NMR (400MHz, CDCl₃): δ 10.68 (s, 1H), 7.89 (d, J=8.0Hz, 1H), 7.51 (s, 1H), 7.30-7.46 (m, 5H), 6.83 (t, J=7.2Hz, 1H), 3.07 (q, 2H), 1.24 (t, J=7.2Hz, 3H); ¹³C NMR (400 MHz, CDCl₃) δ 204.20, 146.57, 141.44, 134.38, 131.59, 129.87, 125.03, 119.78, 119.72, 118.52, 118.49, 117.79, 114.56, 32.70, 8.69. LRMS calculated for C₁₆H₁₅F₃NO⁺ [M+H]⁺, 293.3 found 294.1.

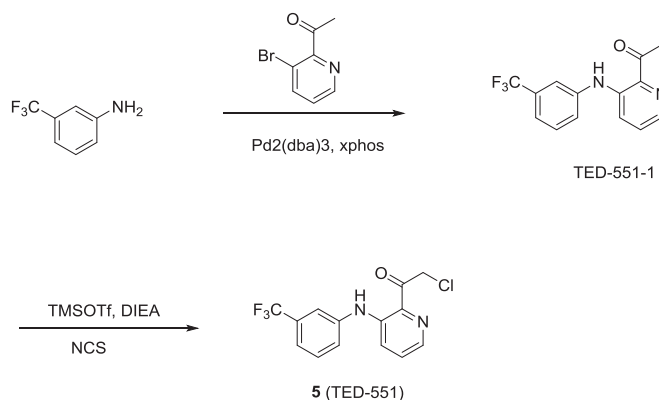
Synthesis Scheme of 4 (TED-548)



Synthesis of 1-(2-((3-(2-methoxyethoxy)phenyl)amino)phenyl)ethanone (TED-548-2). A mixture of 3-(2-methoxyethoxy)aniline (500 mg, 2.99 mmol), 1-(2-bromophenyl)ethanone (625 mg, 3.14 mmol), Pd₂(dba)₃ (275 mg, 0.30 mmol), xphos (286 mg, 0.60 mmol), and Cs₂CO₃ (1.47 g, 4.50 mmol) in dioxane (10 mL) was heated to 90 °C under N₂, and stirred for 2 hr. The reaction mixture was cooled to room temperature, and filtered over Celite. The filtrate was concentrated. The residue was dissolved in EA (40 mL), washed with brine, and dried over Na₂SO₄. The solution was filtered, and the filtrate was concentrated. The residue was purified by column chromatography (PE-PE/EA=5/1) to give 1-(2-((3-(2-methoxyethoxy)phenyl)amino)phenyl)ethanone (710 mg, 83.2%); ¹H NMR (400MHz, CDCl₃): δ 10.51 (s, 1H), 7.81 (d, J=8.0Hz, 1H), 7.30-7.31 (m, 2H), 7.23 (t, J=8.0Hz, 1H), 6.84-6.85 (m, 2H), 6.68-6.76 (m, 2H), 4.11 (t, J=4.8Hz, 2H), 3.75 (t, J=4.8Hz, 2H), 3.45 (s, 3H), 2.64 (s, 3H). LRMS calculated for C₁₇H₂₀NO₃⁺ [M+H]⁺, 286.3 found 286.2.

Synthesis of 2-chloro-1-(2-((3-(2-methoxyethoxy)phenyl)amino)phenyl) ethanone (4, TED-548). To a mixture of 1-(2-((3-(2-methoxyethoxy)phenyl)amino)phenyl)ethanone (50 mg, 0.18 mmol) in DCM (3 mL) were added DIEA (67 mg, 0.52 mmol) and TMSOTf (58 mg, 0.26 mmol) at 0 °C under N₂. The resulting mixture was warmed to room temperature and stirred for 5 hr. NCS (24 mg, 0.18 mmol) was added and the mixture was stirred for another 2 hr. It was quenched with water (10 mL), and the mixture was extracted with DCM (5mL x 3). The organic phase was washed with brine, dried over Na₂SO₄, and filtered. The filtrate was concentrated. The residue was purified by prep. TLC (PE/EA=5/1) to give 2-chloro-1-(2-((3-(2-methoxyethoxy)phenyl)amino)phenyl)ethanone (5.1 mg, 8.9%); ¹H NMR (400MHz, CDCl₃): δ 10.35 (s, 1H), 7.77 (d, J=8.0Hz, 1H), 7.22-7.39 (m, 4H), 7.07 (d, J=2.8Hz, 1H), 6.84 (t, J=7.2Hz, 1H), 6.63-6.65 (m, 1H), 4.76 (s, 2H), 4.08 (t, J=4.8Hz, 2H), 3.74 (t, J=4.8Hz, 2H), 3.45 (s, 3H); ¹³C NMR (400 MHz, CDCl₃): δ 193.13, 157.99, 147.15, 137.90, 135.36, 131.25, 130.56, 117.91, 117.49, 115.51, 110.85, 109.43, 70.95, 67.75, 59.25, 46.55. LRMS calculated for C₁₇H₁₉ClNO₃⁺ [M+H]⁺, 320.8 found 320.0.

Synthesis Scheme of 5 (TED-551)

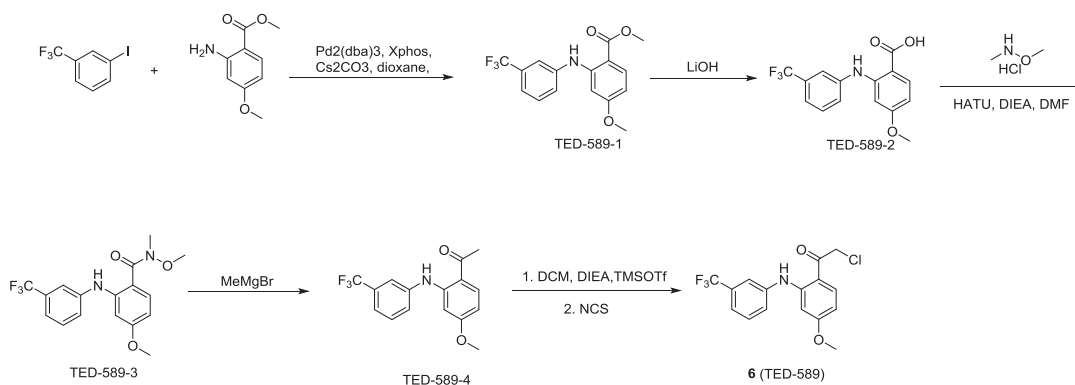


Synthesis of 1-(3-((3-(trifluoromethyl)phenyl)amino)pyridin-2-yl)ethanone (TED-551-1). A mixture of 1-(3-bromopyridin-2-yl)ethanone (200 mg, 1.00 mmol), 3-(trifluoromethyl)aniline (161 mg, 1.00 mmol), Pd₂(dba)₃ (92 mg, 0.10 mmol), xphos (95 mg, 0.20 mmol), and Cs₂CO₃ (489 mg, 1.50 mmol) in dioxane (10 mL) was heated to 90 °C under N₂. The mixture was stirred for 2 hr. The reaction mixture was cooled to room temperature, and filtered through Celite. The filtrate was concentrated. The residue was dissolved in EA (40 mL), and the mixture was washed with brine, dried over Na₂SO₄, and filtered. The filtrate was concentrated. The residue was purified by column chromatography (PE-PE/EA=20/1) to give 1-(3-((3-(trifluoromethyl)phenyl)amino)pyridin-2-yl)ethanone (160 mg, 57.1%); ¹H NMR (400MHz, CDCl₃): δ 10.43 (s, 1H), 8.13 (d, J=4.0Hz, 1H), 7.59 (d, J=8.0Hz, 1H), 7.47-7.51 (m, 2H), 7.39 (t, J=6.4Hz, 2H), 7.26-7.30 (m, 1H), 2.79 (s, 3H). LRMS calculated for C₁₄H₁₂F₃N₂O⁺ [M+H]⁺, 281.3 found 281.1.

Synthesis of 2-chloro-1-(3-((3-(trifluoromethyl)phenyl)amino)pyridin-2-yl)ethanone (5, TED-551). The procedure was the same as 4 (TED-548) to give 5 (TED-551).

5 (TED-551). ¹H NMR (400MHz, CDCl₃): δ 10.21 (s, 1H), 8.11-8.10 (dd, J=4.0Hz, J=1.2Hz, 1H), 7.61-7.58 (m, 1H), 7.53-7.49 (m, 2H), 7.44-7.39 (m, 2H), 7.34-7.31 (m, 1H), 5.20 (s, 2H). ¹³C NMR (400 MHz, CDCl₃): δ 195.58, 143.74, 139.61, 139.07, 133.56, 132.42, 132.10, 130.32, 129.07, 126.07, 125.05, 122.34, 121.64, 121.47, 121.39, 119.51, 119.47, 48.03. LRMS calculated for C₁₄H₁₁ClF₃N₂O⁺ [M+H]⁺, 315.04 found 315.0.

Synthesis Scheme of 6 (TED-589)



Synthesis of methyl 4-methoxy-2-((3-(trifluoromethyl)phenyl)amino)benzoate (TED-589-1). A mixture of methyl 2-amino-4-methoxybenzoate (1.0 g, 5.5 mmol), 1-iodo-3-(trifluoromethyl)benzene (1.8 g, 6.6 mmol), Pd₂(dba)₃ (504 mg, 0.55 mmol), xphos (286 mg, 0.60 mmol), and Cs₂CO₃ (3.6 g, 11.0 mmol) in dioxane (40 mL) was stirred at 90 °C under N₂ overnight. The reaction mixture was cooled to room temperature, and filtered over Celite. The filtrate was concentrated. The residue was dissolved in ethyl acetate (40 mL), washed with brine, and dried over Na₂SO₄. The solution was filtered, and the filtrate was concentrated. The residue was purified by column chromatography (PE-PE/EA=5/1) to give methyl 4-methoxy-2-((3-(trifluoromethyl)phenyl)amino)benzoate (1.12 g, 62.7%); ¹H NMR (400MHz, CDCl₃): δ 9.75 (s, 1H), 7.95-7.92 (d, J=8.8 Hz, 1H), 7.52 (s, 1H), 7.44-7.43 (m, 2H), 7.32-7.30 (d, J=6.8 Hz, 1H), 6.73 (d, J=6.4 Hz, 1H), 6.39-6.36 (dd, J=9.2 Hz, J=2.4 Hz, 1H), 3.88 (s, 3H), 3.76 (s, 3H). LRMS calculated for C₁₇H₂₀NO₃⁺ [M+H]⁺, 326.1 found 326.1.

Synthesis of 4-methoxy-2-((3-(trifluoromethyl)phenyl)amino)benzoic acid (TED-589-2). To a mixture of methyl 4-methoxy-2-((3-(trifluoromethyl)phenyl)amino)benzoate (TED-589-1, 1.12 g, 3.38 mmol) in a mixture of dioxane/water (10 mL/10 mL) was added LiOH.H₂O (1.43 g, 33.8 mmol) at rt and the mixture was stirred for 2 hr. The mixture was acidified to pH 6 with 1 M HCl, and the organic phase was extracted with ethyl acetate (10 mL x 2). The organic phase was washed with brine, dried over Na₂SO₄, and filtered. The filtrate was concentrated. The residue was purified by column chromatography (DCM/MeOH=10/1) to give 4-methoxy-2-((3-(trifluoromethyl)phenyl)amino)benzoic acid (1.07 g, 99% yield); LRMS calculated for C₁₇H₂₀NO₃⁺ [M+H]⁺, 312.1 found 312.1.

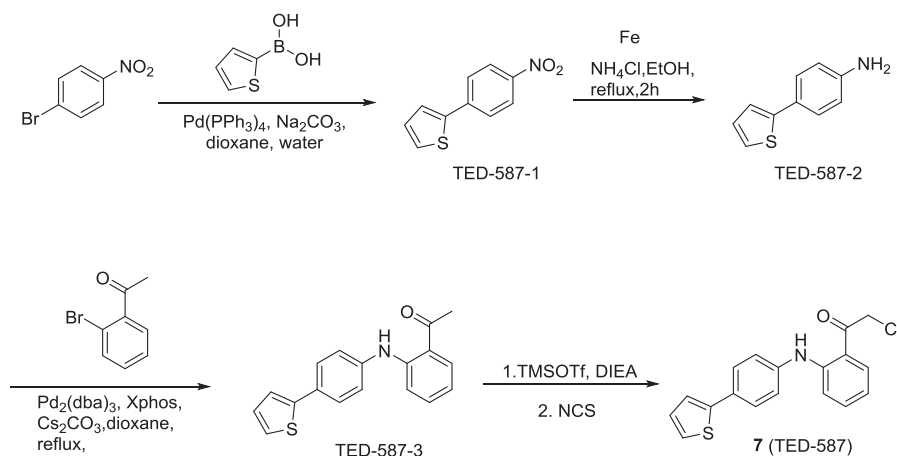
Synthesis of N,4-dimethoxy-N-methyl-2-((3-(trifluoromethyl)phenyl)amino)benzamide (TED-589-3). To a solution of 4-methoxy-2-((3-(trifluoromethyl)phenyl)amino)benzoic acid (TED-589-2, 1.07 g, 3.46 mmol), N,O-dimethylhydroxylamine hydrochloride (503 mg, 5.19 mmol) and HATU (1.97 g, 5.19 mmol) in DMF (20 mL) was added N-ethyl-N-isopropylpropan-2-amine (880 mg, 7.0 mmol). The mixture was stirred at room temperature for 2 hr. After completion of the reaction, ethyl acetate was added to the mixture. Then the mixture was washed with water (100 mL x 2) and brine (100 mL). The organic phase was dried over Na₂SO₄, filtered and concentrated. The residue was purified by column chromatography (PE/EA= 3:1) to give N,4-dimethoxy-N-methyl-2-((3-(trifluoromethyl)phenyl)amino)benzamide as a yellow oil (1.12 g, 91.3 % yield); ¹H NMR (400MHz, CDCl₃): δ 8.44 (s, 1H), 7.54-7.52 (d, J=8.8 Hz, 1H), 7.41-7.40 (d, J=9.2 Hz, 1H), 7.38-7.36 (d, J=8.0 Hz, 1H), 7.29-7.26 (m, 1H), 7.20-7.18 (d, J=7.6 Hz, 1H), 6.88 (d, J=2.8 Hz, 1H), 6.46-6.43 (dd, J=11.2 Hz, J=2.4 Hz, 1H), 3.77 (s, 3H), 3.60 (s, 3H), 3.36 (s, 3H). LRMS calculated for C₁₇H₂₀NO₃⁺ [M+H]⁺, 355.1 found 355.1.

Synthesis of 1-(4-methoxy-2-((3-(trifluoromethyl)phenyl)amino)phenyl)ethanone (TED-589-4). To a solution of N,4-dimethoxy-N-methyl-2-((3-(trifluoromethyl)phenyl)amino)benzamide (TED-589-3, 400 mg, 1.13 mmol) in dry THF (20 mL) under N₂ was added

methylmagnesium bromide (10ml 1.0 M in THF, 10.0 mmol) at 0°C. The mixture was stirred at 0°C for 0.5 hr and then at room temperature for 2 hr. The reaction mixture was quenched by the addition of saturated aqueous NH₄Cl. The organic phase was extracted with ethyl acetate. The combined ethyl acetate layers were washed with brine, dried over anhydrous sodium sulfate, and concentrated. The residue was purified by column chromatography (PE/Ea= 6:1) to give the desired product as a yellow oil (310 mg, 88.5% yield); ¹H NMR (400 MHz, CDCl₃): δ 10.90 (s, 1H), 7.80-7.77 (d, J=8.8 Hz, 1H), 7.55 (s, 1H), 7.46-7.34 (m, 1H), 7.35-7.33 (d, J=6.8 Hz, 1H), 6.70 (d, J=2.4 Hz, 1H), 6.38-6.35 (dd, J=8.8 Hz, J=2.4 Hz, 1H), 3.76 (s, 3H), 2.59 (s, 3H). LRMS calculated for C₁₆H₁₃F₃NO⁺ [M+H]⁺, 310.1 found 310.1.

Synthesis of 2-chloro-1-(4-methoxy-2-((3-(trifluoromethyl)phenyl)amino)phenyl)ethanone (6, TED-589). To a mixture of 1-(4-methoxy-2-((3-(trifluoromethyl)phenyl)amino)phenyl)ethanone (**TED-589-4**, 310 mg, 1.0 mmol) in dichloromethane (DCM) (10 mL) were added DIEA (256 mg, 2.0 mmol) and TMSOTf (266 mg, 1.2 mmol) at 0°C under N₂. The resulting mixture was warmed to room temperature and stirred for 2 hr. NCS (24 mg, 0.18 mmol) was added and the mixture was stirred for another 2 hr. It was quenched with water (10 mL), and the mixture was extracted with DCM (5mL x 3). The organic phase was washed with brine, dried over Na₂SO₄, and filtered. The filtrate was concentrated. The residue was purified by prep. TLC (PE/Ea=5/1) to give the crude product (207 mg). The compound was further purified by reverse HPLC Gilson to afford the desired product as a yellow solid (78 mg, 22.6% yield); ¹H NMR (400MHz, CDCl₃): δ 10.72 (s, 1H), 7.73-7.70 (d, J=9.2 Hz, 1H), 7.56 (s, 1H), 7.50-7.38 (m, 3H), 6.69 (s, 1H), 6.40-6.38 (d, J=8.8 Hz, 1H), 4.67 (s, 2H), 3.77 (s, 3H); ¹³C NMR (400MHz, CDCl₃): δ 191.67, 165.44, 150.50, 140.54, 133.67, 132.44, 132.12, 131.79, 130.11, 126.22, 125.19, 122.49, 120.81, 120.78, 119.66, 119.62, 119.59, 110.91, 105.99, 97.20, 55.37, 46.22. LRMS calculated for C₁₇H₁₉ClNO₃⁺ [M+H]⁺, 344.1 found 344.1.

Synthesis Scheme of 7 (TED-587)



Synthesis of 2-(4-nitrophenyl)thiophene (TED-587-1). A mixture of 1-bromo-4-nitrobenzene (1.0 g, 5.0 mmol), thiophen-2-ylboronic acid (0.64 g, 5.0 mmol), Pd(PPh₃)₄ (580 mg, 0.5 mmol), and Na₂CO₃ (1.1 g, 10.0 mmol) in dioxane (40 mL) and water (5 mL) was stirred at 90°C under N₂ overnight. The reaction mixture was cooled to room temperature, and filtered over Celite. The filtrate was concentrated. The residue was dissolved in ethyl acetate (40 mL), and the solution was washed with brine, and dried over Na₂SO₄. The solution was filtered, and the filtrate was concentrated. The residue was purified by column chromatography (PE-PE/Ea=10/1) to give 2-(4-nitrophenyl)thiophene (0.54 g, 52.6% yield). LRMS calculated for C₁₀H₈NO₂S⁺ [M+H]⁺, 206.0 found 206.0.

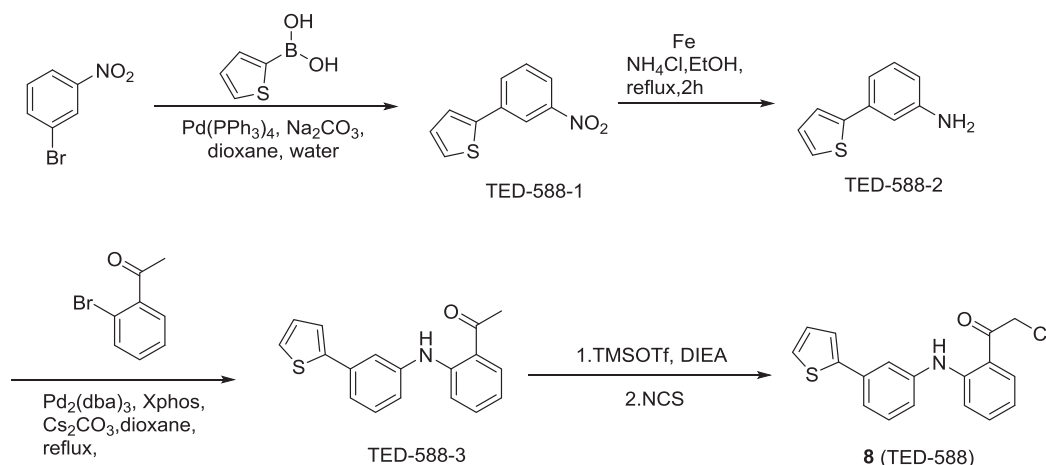
Synthesis of 4-(thiophen-2-yl)aniline (TED-587-2). To a mixture of 2-(4-nitrophenyl)thiophene (540 mg, 2.63 mmol) in EtOH (30 mL) was added sat. NH₄Cl (5 mL), followed by iron powder (740 mg, 13.15 mmol). The resultant mixture was heated to reflux and stirred for 30 min, and then cooled to rt. The mixture was filtered over celite and the filtrate was concentrated. The residue was dissolved in EA. The solution was washed with brine, dried over Na₂SO₄, and filtered. The filtrate was concentrated. The residue was purified by column chromatography (PE/Ea=4:1) to afford 4-(thiophen-2-yl)aniline (360 mg, 78.3% yield). ¹H NMR (400 MHz, CDCl₃): δ 7.42-7.40 (d, J=8.4 Hz, 2H), 7.16-7.15 (m, 2H), 7.03-7.01 (m, 1H), 6.69-6.67 (d, J=8.4 Hz, 2H), 3.72 (br, 2H). LRMS calculated for C₁₀H₁₀NS⁺ [M+H]⁺, 176.1 found 176.1.

Synthesis of 1-(2-((4-(thiophen-2-yl)phenyl)amino)phenyl)ethanone (TED-587-3). A mixture of 4-(thiophen-2-yl)aniline (360 mg, 2.06 mmol), 1-(2-bromophenyl)ethanone (405 mg, 2.06 mmol), Pd₂(dba)₃ (190 mg, 0.21 mmol), xphos (150 mg, 0.32 mmol), and Cs₂CO₃ (1.30 g, 4.0 mmol) in dioxane (30 mL) was stirred at 90°C under N₂ overnight. The reaction mixture was cooled to

room temperature, and filtered over Celite. The filtrate was concentrated. The residue was dissolved in ethyl acetate (40 mL), and the solution was washed with brine, and dried over Na_2SO_4 . The solution was filtered, and the filtrate was concentrated. The residue was purified by column chromatography (PE-PE/EA=8/1) to give 1-(2-((4-(thiophen-2-yl)phenyl)amino)phenyl)ethanone (130 mg, 21.5% yield). LRMS calculated for $\text{C}_{18}\text{H}_{16}\text{NOS}^+ [\text{M}+\text{H}]^+$, 294.1 found 294.1.

Synthesis of 2-chloro-1-(2-((4-(thiophen-2-yl)phenyl)amino)phenyl)ethanone (7, TED-587). To a mixture of 1-(2-((4-(thiophen-2-yl)phenyl)amino)phenyl)ethanone (130 mg, 0.44 mmol) in DCM (10 mL) were added DIEA (120 mg, 0.9 mmol) and TMSOTf (150 mg, 0.66 mmol) at 0°C under N_2 . The resulting mixture was warmed to rt and stirred for 2 hr. NCS (70 mg, 0.53 mmol) was added and the mixture was stirred for another 2 hr. It was quenched with water (10 mL), and the mixture was extracted with DCM (5 mL x 3). The organic phase was washed with brine, dried over Na_2SO_4 , and filtered. The filtrate was concentrated. The residue was purified by prep. TLC (PE/EA=5/1) to give the crude product (207 mg). The compound was further purified by reverse phase HPLC Gilson to afford the desired product as a yellow solid (54 mg, 35.2% yield); ^1H NMR (400 MHz, CDCl_3): δ 10.42 (s, 1H), 7.76-7.74 (d, $J = 8.0$ Hz, 1H), 7.62-7.60 (d, $J = 8.4$ Hz, 2H), 7.39-7.30 (m, 2H), 7.28-7.25 (m, 4H), 7.09-7.07 (dd, $J = 4.8$ Hz, $J = 3.6$ Hz, 1H), 6.79-6.75 (t, $J = 7.2$ Hz, 1H), 4.76 (s, 2H); ^{13}C NMR (400 MHz, CDCl_3): δ 193.05, 148.54, 143.93, 139.12, 135.52, 131.30, 130.60, 128.07, 126.97, 124.50, 123.41, 122.72, 117.00, 116.26, 114.86, 46.62. LRMS calculated for $\text{C}_{18}\text{H}_{15}\text{ClNOS}^+ [\text{M}+\text{H}]^+$, 328.1 found 328.1.

Synthesis Scheme of 8 (TED-588)



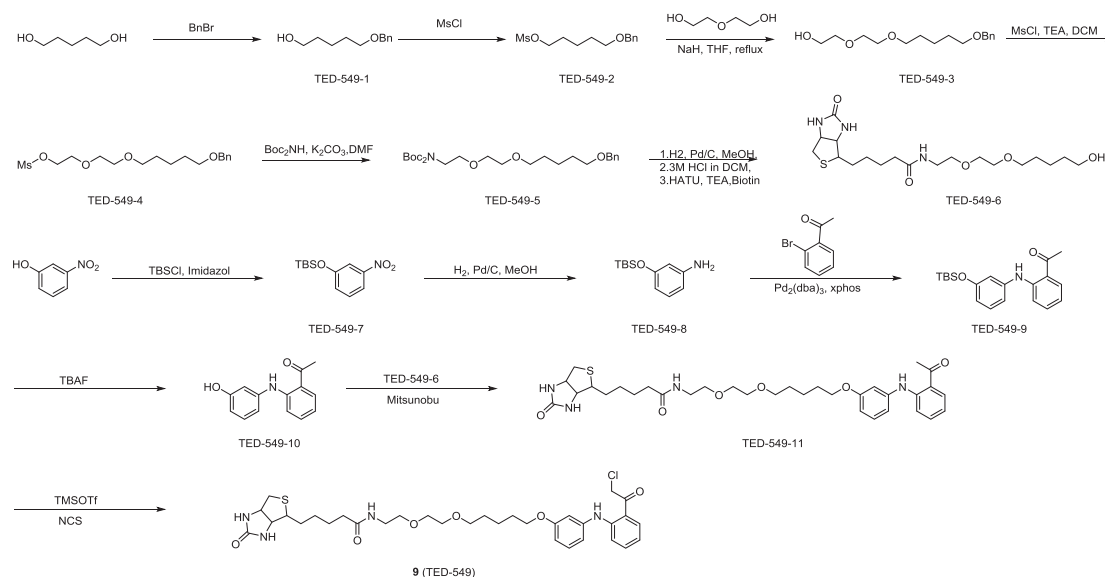
Synthesis of 2-(3-nitrophenyl)thiophene (TED-588-1). The method was the same as **TED-587-1** to give 2-(3-nitrophenyl)thiophene (650 mg, 63.1% yield); ^1H NMR (400 MHz, CDCl_3): δ 8.45 (s, 1H), 8.13-8.11 (d, $J=8.4$ Hz, 1H), 7.92-7.90 (d, $J=7.6$ Hz, 1H), 7.57-7.53 (t, $J=8.0$ Hz, 1H), 7.44 (d, $J=3.6$ Hz, 1H), 7.39 (d, $J=4.8$ Hz, 1H), 7.15-7.13 (m, 1H). LRMS calculated for $\text{C}_{10}\text{H}_8\text{NO}_2\text{S}^+ [\text{M}+\text{H}]^+$, 206.0 found 206.0.

Synthesis of 3-(thiophen-2-yl)aniline (TED-588-2). The method was same as **TED-587-2** to give 3-(thiophen-2-yl)aniline (440 mg, 78.1% yield). LRMS calculated for $\text{C}_{10}\text{H}_{10}\text{NS}^+ [\text{M}+\text{H}]^+$: 176.1, found 176.1.

Synthesis of 1-(2-((3-(thiophen-2-yl)phenyl)amino)phenyl)ethanone (TED-588-3). The method was same as **TED-587-3** to give 1-(2-((3-(thiophen-2-yl)phenyl)amino)phenyl)ethanone (1.4 g, 78.1% yield). LRMS calculated for $\text{C}_{18}\text{H}_{16}\text{NOS}^+ [\text{M}+\text{H}]^+$: 294.1, found 294.1.

Synthesis of 2-chloro-1-(2-((3-(thiophen-2-yl)phenyl)amino)phenyl)ethanone (8, TED-588). The method was same as **7** (TED-587) to give 2-chloro-1-(2-((3-(thiophen-2-yl)phenyl)amino)phenyl)ethanone (27.4 mg, 61.6% yield); ^1H NMR (400 MHz, CDCl_3): δ 10.42 (s, 1H), 7.76-7.74 (d, $J=8.0$ Hz, 1H), 7.49 (s, 1H), 7.40-7.34 (m, 3H), 7.31-7.25 (m, 3H), 7.18-7.17 (d, $J=7.2$ Hz, 1H), 7.09-7.07 (m, 1H), 6.78-6.75 (m, 1H), 4.76 (s, 2H); ^{13}C NMR (400 MHz, CDCl_3): δ 193.09, 148.77, 143.75, 140.36, 135.82, 135.56, 131.30, 129.97, 128.07, 125.51, 123.44, 122.31, 122.09, 116.95, 116.95, 116.20, 114.76, 46.62. LRMS calculated for $\text{C}_{18}\text{H}_{15}\text{ClNOS}^+ [\text{M}+\text{H}]^+$: 328.1, found 328.1.

Synthesis Scheme of 9 (TED-549)



Synthesis of 5-(benzyloxy)pentan-1-ol (TED-549-1). To a solution of pentane-1,5-diol (5.0 g, 48.01 mmol) in DMF (50 mL) was added 60% of NaH (1.3 g, 33.61 mmol) at 0°C under N₂. The resulting mixture was warmed to room temperature and stirred for 30 min. BnBr (5.7 g, 33.61 mmol) was added at 0°C. The mixture was heated to 50°C under N₂, and stirred for 30 min. The reaction mixture was cooled to room temperature, and it was quenched with water (100 mL). The mixture was extracted with EA (40 mL x 3). The organic phase was washed with brine, dried over Na₂SO₄, and filtered. The filtrate was concentrated. The residue was purified by column chromatography (PE-PE/EA=2/1) to give 5-(benzyloxy)pentan-1-ol (2.2 g, 33.7%); ¹H NMR (400MHz, CDCl₃): δ 7.26-7.34 (m, 5H), 4.50 (s, 2H), 3.64 (t, J=6.4Hz, 2H), 3.48 (t, J=6.4Hz, 2H), 1.56-1.67 (m, 4H), 1.41-1.49 (m, 2H), 1.32 (br, 1H).

Synthesis of 5-(benzyloxy)pentyl methanesulfonate (TED-549-2). To a mixture of 5-(benzyloxy)pentan-1-ol (TED-549-1, 2.2 g, 11.32 mmol) in DCM (30 mL) were added MsCl (1.4 g, 12.45 mmol) and TEA (2.3 g, 22.64 mmol) at 0°C under N₂. The resulting mixture was warmed to room temperature and stirred for 1 hr. The reaction mixture was quenched with water (50 mL), and the mixture was extracted with DCM (30mL x 3). The organic phase was washed with brine, dried over Na₂SO₄, and filtered. The filtrate was concentrated to give 5-(benzyloxy)pentyl methanesulfonate (2.5 g, 81.3%); ¹H NMR (400MHz, CDCl₃): δ 7.26-7.35 (m, 5H), 4.50 (s, 2H), 4.23 (t, J=6.4Hz, 2H), 3.48 (t, J=6.4Hz, 2H), 2.99 (s, 3H), 1.76-1.80 (m, 2H), 1.63-1.71 (m, 2H), 1.48-1.54 (m, 2H).

Synthesis of 2-(2-((5-(benzyloxy)pentyl)oxy)ethoxy)ethanol (TED-549-3). To a mixture of 2,2'-oxydiethanol (2.9 g, 27.53 mmol) in THF (50 mL) was added 60% of NaH (550 mg, 13.77 mmol) at 0°C under N₂. The resulting mixture was warmed to room temperature and stirred for 30 min. A solution of 5-(benzyloxy)pentyl methanesulfonate (TED-549-2, 2.5 g, 9.18 mmol) in THF (10 mL) was added and the mixture was refluxed for 3 hr under N₂, and then cooled to room temperature. The reaction mixture was quenched with water (150 mL), and the mixture was extracted with EA (40mL x 3). The organic phase was washed with brine, dried over Na₂SO₄, and filtered. The filtrate was concentrated. The residue was purified by column chromatography (PE/EA=10/1 to 1/1) to give 2-(2-((5-(benzyloxy)pentyl)oxy)ethoxy)ethanol (1.9 g, 73.4%); ¹H NMR (400MHz, CDCl₃): δ 7.26-7.34 (m, 5H), 4.50 (s, 2H), 3.71-3.74 (m, 2H), 3.66-3.69 (m, 2H), 3.57-3.63 (m, 4H), 3.47 (t, J=6.4Hz, 4H), 2.47 (br, 1H), 1.59-1.68 (m, 4H), 1.40-1.47 (m, 2H).

Synthesis of 2-(2-((5-(benzyloxy)pentyl)oxy)ethoxy)ethyl methanesulfonate (TED-549-4). To a mixture of 2-(2-((5-(benzyloxy)pentyl)oxy)ethoxy)ethanol (TED-549-3, 1.9 g, 6.74 mmol) in DCM (50 mL) were added MsCl (0.92 g, 8.09 mmol) and TEA (1.4 g, 13.48 mmol) at 0°C under N₂. The resulting mixture was warmed to room temperature and stirred for 1 hr. The reaction mixture was quenched with water (100 mL), and the mixture was extracted with DCM (30 mL x 3). The organic phase was washed with brine, dried over Na₂SO₄, and filtered. The filtrate was concentrated to give 2-(2-((5-(benzyloxy)pentyl)oxy)ethoxy)ethyl methanesulfonate (1.8 g, 74.1%); ¹H NMR (400MHz, CDCl₃): δ 7.26-7.37 (m, 5H), 4.50 (s, 2H), 4.38 (t, J=4.4Hz, 2H), 3.76 (t, J=4.4Hz, 2H), 3.64-3.66 (m, 2H), 3.56-3.58 (m, 2H), 3.43-3.49 (m, 4H), 3.06 (s, 3H), 1.57-1.65 (m, 4H), 1.38-1.46 (m, 2H).

Synthesis of N,N-diBoc-2-(2-((5-(benzyloxy)pentyl)oxy)ethoxy)ethan-1-amine (TED-549-5). A mixture of 2-(2-((5-(benzyloxy)pentyl)oxy)ethoxy)ethyl methanesulfonate (TED-549-4, 1.8 g, 5.00 mmol), HNBoc₂ (1.2 g, 5.5 mmol) and K₂CO₃ (1.4 g, 10.00 mmol) in DMF (30 mL) was heated to 100°C under N₂ and the mixture was stirred for 3 hr. It was then cooled to room temperature. The reaction mixture was quenched with water (100 mL), and extracted with EA (40mL x 3). The organic phase was washed with brine, dried over Na₂SO₄, and filtered. The filtrate was concentrated. The residue was purified by column chromatography (PE/EA=10/1 to

3/1) to give N,N-diBoc-2-(2-((5-(benzyloxy)pentyl)oxy)ethoxy)ethan-1-amine (2.0 g, 83.1%); $^1\text{H NMR}$ (400MHz, CDCl_3): δ 7.26-7.34 (m, 5H), 4.50 (s, 2H), 3.74-3.80 (m, 2H), 3.53-3.63(m, 6H), 3.42-3.48 (m, 4H), 1.58-1.65 (m, 4H), 1.49 (s, 18H), 1.39-1.45 (m, 2H).

Synthesis of N-(2-(2-((5-hydroxypentyl)oxy)ethoxy)ethyl)-5-(2-oxohexahydro-1H-thieno[3,4-d]imidazol-4-yl)pentanamide (TED-549-6). A mixture of ditert-butyl (2-(2-((5-(benzyloxy)pentyl)oxy)ethoxy)ethyl)carbamate (**TED-549-5**, 2.0 g, 4.15 mmol) and 10% of Pd/C (300 mg) in MeOH (100 mL) was stirred for 18 hr under H_2 . The reaction mixture was filtered through Celite and the filtrate was concentrated. The residue was dissolved in DCM (10 mL) and 6 M HCl in dioxane (5 mL) was added. The resulting mixture was stirred at room temperature for 2 hr and then the solvent was removed. The residue was dissolved in DMF (15 mL), and TEA (1.03 g, 10.02 mmol) was added, followed by HATU (1.16 g, 3.06 mmol). The resulting mixture was stirred at room temperature for 2 hr, and concentrated. The crude product was purified by prep-HPLC to give N-(2-(2-((5-hydroxypentyl)oxy)ethoxy)ethyl)-5-(2-oxohexahydro-1H-thieno[3,4-d]imidazol-4-yl)pentanamide (120 mg, 6.9%); $^1\text{H NMR}$ (400MHz, CD_3OD): δ 4.47-4.50 (m, 1H), 4.29-4.32 (m, 1H), 3.48-3.59 (m, 10H), 3.36 (t, $J=5.6\text{Hz}$, 2H), 3.18-3.23 (m, 1H), 2.90-2.95 (m, 1H), 2.70 (t, $J=12.8\text{Hz}$, 1H), 2.21 (t, $J=7.2\text{Hz}$, 2H), 1.54-1.75 (m, 8H), 1.40-1.48 (m, 4H). LRMS calculated for $\text{C}_{19}\text{H}_{36}\text{N}_3\text{O}_5\text{S}^+$ $[\text{M}+\text{H}]^+$, 418.6, found 418.2.

Synthesis of tert-butyldimethyl(3-nitrophenoxy)silane (TED-549-7). To a solution of 3-nitrophenol (1.0 g, 7.20 mmol) in DCM (20 mL) were added TBSCl (1.2 g, 7.92 mmol) and imidazole (979 mg, 14.40 mmol) at room temperature. The resulting mixture was stirred for 2 hr and quenched with water (40 mL). It was extracted with DCM (30 mL x 3). The organic phase was washed with brine, dried over Na_2SO_4 , and filtered. The filtrate was concentrated. The residue was purified by column chromatography (PE-PE/EA=2/1) to give tert-butyldimethyl(3-nitrophenoxy)silane (1.3 g, 71.4%); $^1\text{H NMR}$ (400MHz, CDCl_3): δ 7.83 (d, $J=8.0\text{Hz}$, 1H), 7.66 (t, $J=2.4\text{Hz}$, 1H), 7.38 (t, $J=8.0\text{Hz}$, 1H), 7.16 (d, $J=8.0\text{Hz}$, 1H), 1.00 (s, 9H), 0.24 (s, 6H), 1.41-1.49 (m, 2H), 1.32 (br, 1H).

Synthesis of 3-((tert-butyldimethylsilyloxy)aniline (TED-549-8). To a mixture of tert-butyldimethyl(3-nitrophenoxy)silane (**TED-549-7**, 1.3 g, 5.14 mmol) in MeOH (20 mL) was added 10% of Pd/C (200 mg). The resulting mixture was stirred at room temperature overnight under H_2 (1 atm). The reaction mixture was filtered through Celite and the filtrate was concentrated to give 3-((tert-butyldimethylsilyloxy)aniline (1.1 g, 95.7%); LRMS calculated for $\text{C}_{12}\text{H}_{22}\text{NOSi}^+$ $[\text{M}+\text{H}]^+$, 224.4, found 224.3.

Synthesis of 1-(2-((3-((tert-butyldimethylsilyloxy)phenyl)amino)phenyl)ethan-1-one (TED-549-9). The mixture of 3-((tert-butyldimethylsilyloxy)aniline (**TED-549-8**, 600 mg, 2.69 mmol), 1-(2-bromophenyl)ethanone (562 mg, 2.83 mmol), $\text{Pd}_2(\text{dba})_3$ (246 mg, 0.27 mmol), xphos (257 mg, 0.54 mmol), and Cs_2CO_3 (1.30 g, 4.04 mmol) in dioxane (15 mL) was heated to 90°C under N_2 , and it was stirred for 2 hr. The reaction mixture was cooled to room temperature, filtered through Celite and the filtrate was concentrated. The residue was dissolved in EA (40 mL), washed with brine, and dried over Na_2SO_4 . It was filtered, and the filtrate was concentrated. The residue was purified by column chromatography (PE-PE/EA=20/1) to give 1-(2-((3-((tert-butyldimethylsilyloxy)phenyl)amino)phenyl)ethan-1-one (410 mg, 44.6%); $^1\text{H NMR}$ (400MHz, CDCl_3): δ 10.47 (s, 1H), 7.81 (d, $J=8.4\text{Hz}$, 1H), 7.28-7.33 (m, 2H), 7.18 (t, $J=8.0\text{Hz}$, 1H), 6.85 (d, $J=7.6\text{Hz}$, 1H), 6.71-6.74 (m, 2H), 6.61 (d, $J=8.4\text{Hz}$, 1H), 2.64 (s, 3H), 0.98 (s, 9H), 0.21 (s, 6H).

Synthesis of 1-(2-((3-hydroxyphenyl)amino)phenyl)ethan-1-one (TED-549-10). To a solution of 1-(2-((3-((tert-butyldimethylsilyloxy)phenyl)amino)phenyl)ethan-1-one (**TED-549-9**, 100 mg, 0.29 mmol) in THF (2 mL) was added 1M TBAF in THF (0.35 mL, 0.35 mmol) dropwise at room temperature. The resulting mixture was stirred for 1 hr and quenched with water (20 mL). The mixture was extracted with EA (10 mL x 3), and the organic phase was washed with brine, and dried over Na_2SO_4 . It was filtered, and the filtrate was concentrated. The residue was purified by prep-TLC (DCM/MeOH=10/1) to give 1-(2-((3-hydroxyphenyl)amino)phenyl)ethan-1-one (52 mg, 70.8%); $^1\text{H NMR}$ (400MHz, CDCl_3): δ 10.49 (s, 1H), 7.82 (d, $J=8.0\text{Hz}$, 1H), 7.32 (d, $J=7.6\text{Hz}$, 2H), 7.20 (t, $J=8.0\text{Hz}$, 1H), 6.83 (d, $J=8.0\text{Hz}$, 1H), 6.73-6.77 (m, 2H), 6.58 (d, $J=8.0\text{Hz}$, 1H), 2.65 (s, 3H). LRMS calculated for $\text{C}_{14}\text{H}_{14}\text{NO}_2^+$ $[\text{M}+\text{H}]^+$, 228.3 found 228.1.

Synthesis of N-(2-(2-((5-(3-((2-acetylphenyl)amino)phenoxy)pentyl)oxy)ethoxy)ethyl)-5-(2-oxohexahydro-1H-thieno[3,4-d]imidazol-4-yl)pentanamide (TED-549-11). To a mixture of N-(2-(2-((5-(benzyloxy)pentyl)oxy)ethoxy)ethyl)-5-(2-oxohexahydro-1H-thieno[3,4-d]imidazol-4-yl)pentanamide (**TED-549-6**, 50 mg, 0.12 mmol), 1-(2-((3-hydroxyphenyl)amino)phenyl)ethan-1-one (**TED-549-10**, 35 mg, 0.16 mmol), and PPh_3 (63 mg, 0.24 mmol) in dioxane (3 mL) was added DIAD (53 mg, 0.26 mmol) at 0°C under N_2 . The resulting mixture was warmed to room temperature and stirred overnight. The reaction mixture was quenched with water (5 mL), and extracted with EA (10 mL x 2). The organic phase was washed with brine, dried over Na_2SO_4 , and filtered. The filtrate was concentrated. The residue was purified by prep-TLC (DCM/MeOH=5/1) to give N-(2-(2-((5-(3-((2-acetylphenyl)amino)phenoxy)pentyl)oxy)ethoxy)ethyl)-5-(2-oxohexahydro-1H-thieno[3,4-d]imidazol-4-yl)pentanamide (42 mg, 46% yield); $^1\text{H NMR}$ (400MHz, CDCl_3): δ 10.50 (s, 1H), 7.81 (d, $J=8.0\text{Hz}$, 1H), 7.26-7.34 (m, 2H), 7.12-7.24 (m, 1H), 6.72-6.85 (m, 2H), 6.63-6.66 (m, 1H), 6.48-6.58 (m, 1H), 6.12 (s, 1H), 5.22 (s, 1H), 4.86-4.97 (m, 1H), 4.46-4.49 (m, 1H), 4.28-4.31 (m, 1H), 3.88-3.96 (m, 2H), 3.44-3.64 (m, 10H), 3.10-3.14 (m, 1H), 2.87-2.91 (m, 1H), 2.70-2.74 (m, 1H), 2.64 (s, 2H), 2.15-2.26 (m, 2H), 1.56-1.84 (m, 12H). LRMS calculated for $\text{C}_{33}\text{H}_{47}\text{N}_4\text{O}_6\text{S}^+$ $[\text{M}+\text{H}]^+$, 627.3 found 627.4.

Synthesis of N-(2-(2-((5-(3-((2-chloroacetyl)phenyl)amino)phenoxy)pentyl)oxy)ethoxy)ethyl)-5-(2-oxohexahydro-1H-thieno[3,4-d]imidazol-4-yl)pentanamide (9, TED-549). The method was the same as **4** (TED-548) to give N-(2-(2-((5-(3-((2-chloroacetyl)phenyl)amino)phenoxy)pentyl)oxy)ethoxy)ethyl)-5-(2-oxohexahydro-1H-thieno[3,4-d]imidazol-4-yl)pentanamide (11 mg); $^1\text{H NMR}$ (400MHz, CDCl_3): δ 10.33 (s, 1H), 7.71-7.80 (m, 2H), 6.72-6.85 (m, 4H), 6.60-6.62 (m, 3H), 6.30-6.39 (m, 2H), 5.44 (s, 2H), 4.88-5.09 (m, 3H), 4.76 (s, 2H), 4.70 (s, 1H), 4.47 (s, 2H), 4.29 (m, 2H), 3.92-4.00 (m, 5H), 3.43-3.60 (m, 25H), 3.05-3.15 (m, 2H), 2.86-2.91 (m, 2H), 2.65-2.74 (m, 3H), 2.21 (br, 6H). LRMS calculated for $\text{C}_{33}\text{H}_{46}\text{ClN}_4\text{O}_6\text{S}^+$ $[\text{M}+\text{H}]^+$, 661.3, found 661.2.

QUANTIFICATION AND STATISTICAL ANALYSIS

Fluorescence polarization, biolayer interferometry, and cell biological studies results are representatives of at least three independent studies, performed in duplicates.

Crystal structure statistics are available in [Table S2](#).

DATA AND SOFTWARE AVAILABILITY

The accession number for the atomic coordinates of human TEAD2 Yap-binding domain covalently bound to compound **2**, reported in this paper, is PDB: 6E5G.

ADDITIONAL RESOURCES

N/A.